Synergy of chemotherapy and macrophage depletion leads to T cell memory activation and durable triple negative breast cancer regression

Swarnima Singh[1,2], Nigel Lee[3], Igor Bado[1], Clark Hamor[1], Licheng Zhang[6], Sergio Aguirre[1], Jingyuan Hu[3], Yichao Shen[1], Yitian Xu[6], Yang Gao[1], Diego Pedroza[1], Na Zhao[1], Shu-Hsia Chen[6], Ying-Wooi Wan[3], Zhandong Liu[3], Jeffrey T. Chang[4], Daniel Hollern[7], Charles M. Perou[5], Xiang H.F. Zhang[1,2*], Jeffrey M. Rosen[1,2*]

1. Department of Molecular and Cellular Biology and Dan L Duncan Comprehensive Cancer Center, Baylor College of Medicine
2. Translational Biology and Molecular Medicine, Baylor College of Medicine
3. Jan and Dan Duncan Neurological Research Institute at Texas Children's Hospital, Houston, United States
4. Department of Integrative Biology and Pharmacology, The University of Texas Health Science Center at Houston.
5. Lineberger Comprehensive Cancer Center, University of North Carolina, Chapel Hill, NC 27599, USA
6. Immunominotoring Core, Center for Immunotherapy Research, Houston Methodist Research Institute (HMRI), 6670 Bertner Avenue, R9-330.11, Houston, Texas 77030
7. Salk Institute for Biological Studies, Salk Cancer Center, NOMIS Center for Immunobiology and Microbial Pathogenesis, 10010 N Torrey Pines Rd • La Jolla, CA 92037

*-Co-corresponding authors

Abstract

Abstract

Immunosuppressive elements within the tumor microenvironment such as Tumor Associated Macrophages (TAMs) can present a barrier to successful anti-tumor responses by cytolytic T cells. We employed preclinical syngeneic p53 null mouse models of TNBC to develop a treatment regimen that harnessed the immunostimulatory effects of low-dose chemotherapy coupled with the pharmacologic inhibition of TAMs. Combination therapy was used to successfully treat several highly aggressive, claudin-low murine mammary tumors and lung metastasis. Long-term responders developed tertiary lymphoid structures co-infiltrated by T and B cells at the treatment site. Mechanistically, CD86+ antigen-experienced T cells exhibited polyclonal expansion and resulted in exceptional responses upon tumor rechallenge. Combination treatment also eliminated lung metastases. High dimensional transcriptomic data for CD45+ immune cells lead to the identification of an aberrant developmental trajectory for TAMs that were resistant to treatment. Signatures derived from these TAM populations were predictive of patient response to our therapy. This study illustrates the complexity of tumor infiltrating myeloid cells and highlights the importance of personalized immuno-genomics to inform therapeutic regimens.

Statement of significance

Triple negative breast cancer is aggressive and hard to treat as it has no targeted therapies. Targeting immunosuppressive macrophages in murine models of TNBC alongside an immunostimulatory chemotherapy achieved long-term primary tumor regression in multiple murine mouse models. The transcriptomic heterogeneity between TAMs in phenotypically similar models can be used to uncover future therapeutic targets. Additionally, signatures derived from these murine models can be applied to TNBC patient data sets to predict cohorts of patients that will respond to the treatment strategy.

Introduction

Heterogeneity in TNBC has been well characterized with respect to cancer cell intrinsic features (1), but much less is known about the contribution of tumor infiltrating immune cells. Immunologically hot tumors that are associated with a better prognosis have a high infiltration of CD8+ T cells; however not all tumors respond equally to checkpoint blockade. Immunosuppressive myeloid cells such as TAMs have been implicated in suppressing anti-tumor T cell responses and promoting angiogenesis, tumor invasion, extravasation and metastasis within the dynamic tumor immune microenvironment (TIME) and TNBC patients with a high TAM signature have a poor prognosis.

We have developed novel preclinical p53 -/- syngeneic TNBC GEM models including several with a high mutation burden and sensitivity to IO (2, 3), and others that are highly sensitive to specific chemotherapeutic agents (i.e., CTX or carboplatin (4, 5)). These unique syngeneic GEM models have been genomically profiled (6, 7), and more recently characterized with respect to the immune microenvironment (8). Furthermore, we have studied their responses to IO and validated these results in human patient datasets (2).

Single-cell RNA sequencing as well as profiling of TCR repertoires have proven to be valuable tools to dissect the cellular heterogeneity in various cancers. By combining high dimensional transcriptomic data of individual tumor infiltrating immune cells with bulk RNA sequencing data from the multiple murine mammary tumor models, we have begun to identify the complex dynamics that prevent tumors from undergoing long-term regression in order to uncover additional targets to overcome treatment resistance. Furthermore, we have harnessed the immunostimulatory effects of the low-dose chemotherapeutic agent cyclophosphamide (Cytoxan, CTX) aided by the depletion of immunosuppressive TAMs (Pexidartinib, PXB) to successfully induce durable long-term responses in highly aggressive primary murine mammary tumors. The presence of tertiary lymphoid structures has been associated with responders to checkpoint blockade (9), and we observed TLS infiltrated by antigen experienced CD127+ CD8+ memory T cells and CD19+ B cells in responders to this combination treatment regimen. We also characterized TAM populations in a phenotypically similar, but recurrent mouse model that may provide useful clues to understand TAM heterogeneity and develop future therapeutics targeting TAM metabolism. Finally, we have shown that combination therapy also can reduce established lung metastasis. These studies highlight the importance of identifying specific biomarkers to predict patient responses to this treatment combination.

Results

p53 -/- syngeneic TNBC GEM recapitulate human TNBC subtypes and respond to low dose immunostimulatory chemotherapy treatment

A screen using “standard of care” drugs on a claudin-low p53 null syngeneic GEM model of TNBC T11 showed that these tumors were resistant to most conventional chemotherapy treatments but responded to low-dose cyclophosphamide (10) (CTX,100mg/kg) treatment (Fig S1a). We utilized another closely related claudin-low model, T12, to understand the basis for this response. These tumors have an enrichment for the EMT pathway (Fig 1a) and also are highly infiltrated by TAMs (Fig 1b, Fig S1b) when compared to other more basal-like or luminal p53 -/- tumor models such as 2225L and 2208L. Principal component analysis also showed that the 3 claudin-low tumor models clustered together as compared to tumor models from basal(2225L) and luminal(2208L) subtypes, indicating a certain degree of transcriptomic similarity between these models (Fig 1c).

Interestingly, T12 tumors implanted in the mammary fat pads of Balb/c mice showed a greater decrease in tumor volume as compared to NSG mice that lack T Cells, B Cells and functional NK cells (Fig 1d) suggesting a possible synergy between T cells and CTX or its analogues was required for superior T12 tumor cell killing. This was supported by in-vitro assays using GFP targeting T Cells derived from JEDI mice (11) that showed a significant increase in cell death of GFP+ T12 cells upon addition of an active metabolite of CTX, phosphoramide mustard (PM) (Fig 1e). Furthermore, flow cytometry analysis revealed an increase in the numbers of CD4+ and CD8+ T cells in T12 tumors after CTX treatment in immunocompetent Balb/c mice (FigS1c, S1e). Antibody depletion of CD4+ resulted in an impaired response to CTX (Fig 1f) but did not fully abolish the differences in response between of Balb/c mice compared to NSG mice indicating there is a synergy between the T cell subtypes that promotes tumor regression. Additionally, an enrichment in TAMs as well as lower numbers of CD8+ T cells (Fig S1d, S1f, 1g) was observed in the tumors after the depletion of CD4+ T Cells. As CTX treated tumors always recurred after treatment cessation, we then asked if TAMs mediated the resistance to CTX treatment, and if so whether a treatment targeting TAMs would synergize with low-dose CTX and lead to a durable tumor response.

We implanted three independent claudin-low p53 null tumor models T11, T12 and 2151R that have been shown to have a high TAM infiltration and enrichment for the EMT pathway (Fig 1a, 1b) into the mammary fat pads of immunocompetent Balb/c mice. The tumors were allowed to reach a size of approximately 5 mm in diameter and were then randomized into four treatment groups-PBS, CTX, Pexidartinib (PXB) and CTX + PXB (Fig 1g). PXB is a novel small molecule inhibitor of CSF1R, which is a well-known macrophage recruitment and differentiation factor (12) as well as an inhibitor of C-KIT and FLT3 (13). PXB recently gained FDA approval to treat TNGCT (14) and has been widely used in preclinical studies to deplete TAMs. However, PXB has failed to show efficacy as a single agent, and this led us to test this agent in combination with CTX (Fig 1g).

Combination treatment led to long term durable regression in two out of three tumor models namely T12 and 2151R as well as tumor stasis in T11(Fig 1h, 1i, 1j). Excitingly, no tumors recurred in T12 while one out of eight tumors recurred in 2151R within 30 days after treatment cessation (Fig 1k,1l). In contrast, all T11 tumors grew back upon treatment cessation (Fig 1m). Flow cytometry analysis also revealed that combination therapy treated tumors had a significant enrichment of CD8+ T cells that expressed T central memory such as CD62l and CD127 as compared to single agent treated tumors and also an increase in CD8+ effector memory T cells (CD62L+CD127+CD44+) (Fig S1h, S1i).

Finally, we used reduced (3.3 X lower dose) of PXB in combination with CTX as Csf1r inhibitors may elicit liver toxicity (33). The low-dose combination treatment also yielded a significant survival benefit for primary tumors as compared to single agent treated T12 tumors (Fig S1j).

Imaging Mass Cytometry and Single cell RNA sequencing show that combination treatment can lead to an expansion of CD8+/CD4+ T cells and B cells in responsive T12 tumors

Spatial analysis done in TNBC has shown that tumors with a high number of CD8+ T cells that infiltrate into the tumor core have more favorable prognosis as compared to stroma restricted cells, indicating the importance of understanding the TIME architecture with respect to immune cells (15). Accordingly, we performed high dimensional imaging mass cytometry on T12 and T11 tumors before and after treatment. T12 tumors that were treated with combination therapy had larger numbers of CD8+/CD4+ T cells surrounded by clusters of B220+ B cells and CD11C+ CD86+ Dendritic cells (Fig 2a, 2b, 2c, 2d, 2e) while T11 tumors were populated by PANCK+ proliferating (Ki67+) tumor cells and LY6G+PDL1+ granulocytes interacting with sub-populations of CD8+ and CD4+ T cells (S2a, S2b, S2c). T12 tumors treated with CTX alone had the highest number of CD11B+ F480+ TAMs (Fig 2a, S2c) surrounding CD8+/CD4+ T cells (Fig 2c, 2d, 2e) and a paucity of B220+ B cells (Fig 2d, S2c), which may potentially explain the reduced response to this drug after 6 treatments. Previously we have shown a decrease in TAMs after a 3-week CTX treatment course (Fig S1f)-indicating the TAMs that persist after 6 treatments are resistant to CTX alone.

To further elucidate the immune effects of low dose CTX on TNBC, we performed scRNAseq and VD(J) seq on CD45+ cells isolated from T12 tumors before and after treatment (Fig 2f). Uniform Manifold Approximation and Projection (UMAP) projections of the cells revealed 27 different clusters of immune cells across the 4 different treatment groups (Fig 2g, 2h) including CD68+ TAMs, S100a8+ Neutrophils, CD19+ B cells as well as CD8+ and CD4+ T cells (Fig 2i, 2j, S2d). A nearly complete depletion of TAMs in the combination treated group was observed as well as a significant expansion of CD4+ and CD8+ T cells (Fig 2h, 2i). PXB alone tumors had high levels of S100A8+ neutrophils (2i, 2j) supporting previous studies done by our laboratories showing the accumulation of tumor infiltrating neutrophils (TINs) upon TAM depletion in treatment refractory mice (8). To further understand T cell functionality in the absence of immunosuppressive TINs and TAMs after combination treatment, we focused our analysis on the single cell sequencing and V(D)J data for CD8+ T cells in all 4 treatment groups.

Combination therapy treated T12 tumors are infiltrated by polyclonally expanded, less differentiated, exhaustion resistant CD8+ CD127+ memory T cells.

The reclustering of 2346 CD8+ T cells (see Methods) from all 4 treatment groups, revealed 6 different clusters of T cells including Smad7+ Naïve CD8+ T, Nfκbia+ CD8+ T central memory/memory precursors, Ly6a CD8+ T central memory, Gzmb+ CD8+ T effector, Mki67+ CD8+ T proliferative and Lag3+ exhausted CD8+ T cells (Fig 3a, S3a, S3b). CD8+ T central memory cells were greatly increased after combination therapy as compared to the other sub-populations of T cells (Fig 3b, 3c). Pseudotime analysis by Monocle3 (16) revealed that these cells were less differentiated as compared to other groups (Fig 3d). CD8+ Tcm/scm cells marked by the expression of CD62l+ and CD127+(Il7R) (S3b, S3c) in the combination treated group expressed high levels of markers such as Jun, Id3 (17) and Nfκbia (Fig 3e) which are markers of exhaustion resistance (18), longevity (17) and are required for the maintenance of secondary lymphoid structures (19). Additionally, these cells expressed markers of early activation such as Cd28 and Cd69 that also control T cell differentiation (20) (S3c). Consistent with these results, combination treated CD8+ T cells also had a low expression of terminal exhaustion markers such as Pdcd1, Lag3 and Tigit as compared to those in untreated or single agent treated mice (Fig 3e). Thus, scRNA-seq analyses confirmed flow cytometry results and revealed a profound expansion of long-lived, CD8 + memory T cells upon combined PXB and CTX treatment, which may explain the durable responses for up to 60 days post-treatment seen in this group.

Most anti-tumor responses by CD8+ T cells are due to their clonal expansion triggered by specific tumor antigens that are presented by antigen presenting cells (APCs) such as CD11C+ dendritic cells and B220+ B cells (21). Macrophages can present antigens as well but cannot infiltrate lymph nodes or secondary lymphoid structures, that are usually the sites of antigen presentation (22). In these experiments, exhausted CD8+ T cells in PBS and CTX treated groups revealed had higher clonality, which is in line with studies showing monoclonal enrichment of exhausted T cells after checkpoint blockade (23). However, the T cells in the

combination treated group showed a polyclonal expansion with no enrichment for a single clone (Fig 3f, 3g) This diverse response could be due to a phenomenon called “epitope spreading” where T cells can target multiple epitopes of the same antigen or multiple neoantigens (24).

Studies have shown that cytokine stimulation of naïve CD8+ T cells can generate CD8+Tcm cells that do not require antigen presentation. Further studies need to be done to determine whether the polyclonal expansion of CD8+ T cells is due to the presence of many tumor associated neoantigens, if different TCRs can recognize the same tumor antigen or if the expansion is due to the secretion of cytokines by other cells within the TME.

Excitingly, re-challenging these mice with T12 tumors in the contralateral mammary gland led to complete tumor rejection in 40% of the mice and partial rejection in an additional 20% of the cohort (Fig 3h, 3i). This result again supports that the combined treatment establishes long-term immune memory against tumor cells.

Tertiary Lymphoid Structures (TLS) infiltrated by antigen experienced CD127+ CD8+/CD4+ memory T cells and antigen presenting B220+ B cells and CD11C+CD86+ dendritic cells are observed in the tumor beds of long-term responders.

Consistent with this long-lasting durable response to combination treatment, we observed the presence of tertiary lymphoid structures (TLS) in the tumor beds of treated mice bearing regressed T12 tumors. Since TLS have been implicated in improved responses to checkpoint blockade therapy (9), we performed high dimensional imaging analysis on these structures (Fig 4a,4b). Spatial analysis of these structures revealed significant interactions between subsets of CD8+/CD4+ memory T cells and APCs (B cells and Dendritic cells) and avoidance of CD11b+ F480+ macrophages (Fig 4c,4d). We also observed the presence of CD86+CD244+ antigen-experienced T cells as well as CD127+ memory T cells (Fig 4e, Fig S4b) that corroborated the results of our single cell RNA sequencing analysis and suggested the possibility of antigen presentation and T cell activation taking place within tertiary lymphoid structures.

Next, we focused on CD4+ T cells and their roles in the long-term response to combination therapy, since CD4+ T cell depletion blunted responses to CTX and enriched TAMs. Single cell sequencing showed significantly higher numbers of infiltrating CD4+ T cells in combination treated T12 tumors (Fig 2i). We further characterized these cells and noted the expression of activation markers such as CD69 and CD28 (Fig 4f, 4g). Earlier, we had shown that CD19+ B cells were enriched in combination treated tumors as compared to CTX alone and we observed the expression of high levels of MHCII (H2-Ab1) on these cells, which is required for antigen presentation to CD4+ T cells (Fig S4d). Furthermore, we observed high expression of the CD40 ligand on combination treated CD4+ T cells while the combination treated B cells preferentially expressed higher levels of CD40 (Fig 4d,4e). This suggests a possible mechanism for the development of CD4+ T cell effector and memory functions and reciprocal benefits that could promote B cell development and homeostasis via the CD40-CD40L signaling axis (25). Further studies are warranted to study the effects of CD40 agonists or antagonists on treatment response.

The variable responses of three different models (Fig. 1h-j) suggest mechanisms regulating different degrees of sensitivity. We examined cytokines and chemokines in bulk RNA seq data for T11, T12 and 2151R tumors to look for similarities between the 2 responsive models. We saw that Il7 was significantly enriched in both T12 and 2151R tumors (Fig S4e) and this was validated by qPCR (Fig S4f), indicating that these 2 tumors models might have more favorable environments for T cell expansion and maintenance. However, the high levels of F480+ TAMs in CTX treated T12 tumors that were recurrent led us to look into the accumulation of TAMs in treatment resistant T11 tumors. We focused our analysis on the CD68+ myeloid cells in untreated T12 and T11 tumors models to understand the differences between the 2 TAM populations and derive signatures that might potentially stratify TNBC patients into different prognostic groups.

Single cell RNA sequencing and IMC reveal phenotypically similar (CD68+, F480+) but transcriptomically distinct TAMs in responsive(T12) and non-responsive(T11) tumors.

There are many genetic and phenotypic similarities between the T12 and T11 p53 null tumor models. Bulk RNA sequencing revealed an enrichment for the EMT pathway and a claudin low phenotype (1) as well as an

increased infiltration by TAMs. Therefore, the lack of durable response in T11 tumors came as a surprise and led to the question why these genetically and phenotypically similar models displayed a differential response. To address this question, we performed scRNA seq on untreated T11 and T12 CD45+ immune cells. TAMS clustered into 18 Seurat clusters (Fig 5a, S5a). Interestingly the majority of the macrophage populations for these tumor models did not overlap, indicating a degree of heterogeneity in the CD68+ myeloid cell populations in these tumors (Fig 5b). Pseudotime analysis showed T11 AND T12 TAMs follow distinct developmental trajectories with T11 TAMs being less differentiated as compared to T12 TAMs- resulting in unique populations of TAMs expressing genes such as S100a4, Mrc1(CD206) and C1qb (Fig 5c, S5d). The baseline expression of CSf1r was similar in both of these tumor models (Data not shown), indicating the possibility that the T11 TAMs differentiation status might enable them to switch to different pathways for their recruitment and survival upon CSF1R inhibition. Interestingly, Mrc1 is a known marker of immunosuppressive M2 TAMs, and more T12 TAMs expressed higher levels of this marker as compared to T11 TAMs, however in vitro co-culture assays revealed both these TAM populations were equally immunosuppressive (Fig S5d). This highlights the importance of using high dimensional data to identify cellular sub-populations instead of relying only on a few phenotypic markers.

IMC for T12 and T11 tumors post combination therapy shows a significantly increased population of Ki67+ proliferating cells as well as stromal cells in T11 tumors that did not respond to therapy. Additionally, the CD8+ T cells were relegated to the tumor periphery and were surrounded by F480+ TAMs that sequestered them from Ki67+ tumor cells (Fig S5a, S5b). Treated T12 tumors however had fewer numbers of Ki67+ proliferating cells and the CD8+ T cells that had infiltrated the tumor bed were in close contact with the reminder of those cells, suggesting contact dependent killing of tumor cells (Fig 2d).

Accordingly, we performed pathway analysis on T11/T12 TAMs. This analysis revealed a distinct enrichment of pathways in these two models. T12 tumors were enriched in pathways related to macrophage activation and showed a dependence on glycolysis while T11 TAMs expressed high levels of metabolic pathways including oxidative phosphorylation (Fig 5E). Additionally, T12 TAMs were more similar to LPS activated monocytes (26) while T11 TAMs expressed genes similar to anti-inflammatory TAMs (27) (Fig 5e). These results illustrate the necessity for more refined proteomics and genomics to better define the heterogenous nature of TAMs that might appear to be phenotypically similar by analyzing only the canonical surface markers such as F4/80 and CD68. Interestingly, bulk RNA seq data for T11 and T12 tumors did not reveal an enrichment in the oxidative phosphorylation pathway-indicating that there might be a level of specificity for this enrichment in T11 TAMs (Fig 1a).

Survival analysis of TNBC patient datasets reveal different prognosis for patients with high T12 or T11 signature before or after chemotherapy.

The availability of two tumor models that exhibited differential responses lead us to derive signatures from the scRNA seq data for these tumors. Differentially expressed genes were obtained for the TAM subsets from T11 and T12 scRNA seq data (Fig 5c) and these signatures were then applied to bulk RNA sequencing datasets for various p53 null mouse models. scRNA seq derived signatures showed a high level of concordance with their bulk RNA seq counterparts indicating that the signatures derived from scRNA sequencing data can potentially be used to interrogate already existing bulk RNA seq data from patients (Data not shown).

To demonstrate the translational relevance of these signature, we applied them to human patient datasets for patients with TNBC. Survival analysis on a METABRIC dataset showed that a high T12 signature was associated with significantly higher overall survival for TNBC patients treated with chemotherapy while a high T11vsT12 signature offered no such benefits (Fig 6 a, b, c). In fact, a high T11 signature was associated with significantly lower OS rates in patients across all the breast cancer subtypes (Fig S6a). We also checked these signatures in a publicly available RNA sequencing dataset for TNBC patients (52). In this study, core biopsies were collected from BC patients including those with TNBC at different timepoints-T1-pre-NAC (Neoadjuvant chemotherapy) and while they were on NAC(T2). We observed an association with an increase in the T12 vsT11 signature in patients that obtained pCR after AC (Adriamycin + Cyclophosphamide) treatment whereas there was no increase in the T11vsT12 signature. However, T11 signatures significantly increased in patients

with residual disease after chemotherapy (Fig 6d). This suggests that the population of residual TAMs after chemotherapy might be more immunosuppressive and require additional therapies to improve patient outcomes. Residual disease after neoadjuvant chemotherapy usually correlates with lower 5-year event-free survival rates and an increased frequency of metastasis (30). These findings suggest an association between the T12 TAM signature and a positive clinical outcome. The increased expression of the T11 signature in patients with residual disease warrants further investigation into identifying unique markers to target these macrophage sub-populations.

Combination therapy can be used to treat T12 lung metastasis.

Approximately 46% of patients with TNBC will develop distant metastasis and these patients have a median survival of only 13.3 months (31). Therefore, there is an urgent need for treatments that might be effective on established metastases. To this end, we injected via the tail vein T12 tumor cells into Balb/c mice. The mice were randomized onto treatment groups at day 10 after the injection (Fig 6c). CTX alone and combination therapy had a dramatic effect on the reduction of lung lesions as compared to PBS or PXB treated groups-with combination therapy showing a significant advantage over the CTX alone cohort (Fig 6d, 6e). Interestingly, treatment with PXB alone resulted in an increased metastatic burden consistent with previous studies on the role of Csf1r in claudin-low tumor cells (32). Further studies will be required to determine whether combination treatment leads to a durable regression of metastatic lesions following treatment cessation.

Discussion

Triple negative breast cancer is a highly aggressive malignancy with higher rates of occurrence in young as well as African American women (34). Current treatment usually employs cytotoxic chemotherapies. While certain clinical trials have reported positive outcomes for TNBC including T cell activating agents such as checkpoint inhibitors, the response rates in these patients vary and clearly more refined therapies are needed to improve patient survival especially in the metastatic setting (35). The immune microenvironment in TNBC has been suggested to play a critical role in patient response. Accordingly, our laboratories have extensively characterized the immune microenvironments of various GEM TNBC models including those that are either neutrophil enriched or macrophage enriched and have begun to decipher the molecular mechanisms behind how different immune cells are recruited to both the primary tumor and metastasis (8).

In this study, we performed an in-depth analysis of claudin-low TNBC using the latest single cell RNA and VDJ seq techniques as well as sophisticated imaging technologies such as Imaging Mass Cytometry. These tools have provided new insights into changes in the immune microenvironment before and after combination treatment with both chemo- and macrophage- targeting therapies. Surprisingly, these studies revealed a subtle heterogeneity that exists between genetically and phenotypically related models that appear to be enriched for similar immune cells types such as macrophages and pathways such as the EMT pathway (1). The models used in this study, namely T12, T11 and 2151R have shown varying responses to a low dose CTX and a FDA approved Csf1r inhibitor. While T12 and 2151R models display a dramatic response leading to as complete long-lasting regression of the primary tumors upon treatment cessation, T11 tumors display stasis while undergoing treatment but recurred rapidly once treatment cessation. Thus, depletion of TAMs within the tumor microenvironment coupled with a low dose of immunostimulatory chemotherapy was able to elicit durable tumor regression and an expansion of long-lived central memory T cells in certain TAM infiltrated models. These cells persist for long periods of time at the primary tumor site after tumor regression and they may also facilitate tumor rejection upon rechallenge. Another unexpected observation is the presence of Tertiary Lymphoid Structures within the primary tumor site that persist post treatment. While these structures have been implicated in improving the prognosis for patients that respond to checkpoint inhibition (9)-they are usually thought to be transient and have not been studied in detail in mouse models of TNBC. We have shown that TLS co-infiltrated by B cells and memory T cells can persist within the tumor site for extended periods of time. Signatures derived from these models are able predict patients with residual disease that might potentially benefit from this treatment prior to surgery or possibly even during recurrence and metastasis.

One potential advantage of using preclinical models is to improve therapeutic regimens that very often lead to serious adverse events in patients that might be irreversible and cause long-lasting damage (33). Accordingly, we coupled our low dose CTX with a lower dose of PXB and still observed a dramatic regression of primary tumors with this combination therapy. This illustrates the potential efficacy of drug combinations given at less than the maximum tolerated dose, but rather at a minimal effective dose. However, this approach remains to be validated in clinical trials.

Tumor associated macrophages classically have been classified as either M1 and M2 type macrophages with activating and immunosuppressive functions, respectively although more recent studies have illustrated that this designation is overly simplified and there is a much more complex spectrum of activities (36). Studies that have performed single cell RNA sequencing on patients with colorectal cancer have identified subsets of C1QB+ macrophages that have differential sensitivity to CSF1R blockade (37). These results are consistent with our data that shows T12 TAMs have high C1QB and are more sensitive to inhibition. Conversely the T11 TNBC model is infiltrated by highly metabolically active TAMs that are marked by the expression of S100a4 and Acp5. Additionally, while T12 TAMS appear to have an increase of the glycolytic pathway T12 TAMs seem to depend upon oxidative phosphorylation for their energy needs. This suggests that further studies done using inhibitors of oxidative phosphorylation and the electron transport chain in this model are warranted. For example, a small molecule inhibitor of oxidative phosphorylation-IMT1B (38)-has shown some efficacy in models of human ovarian cancer and could potentially be an interesting drug to combine with immunostimulatory chemotherapy. This may target this subset of TAMs and potentially might result in a durable long-term tumor response. Another drug is Venetoclax- a known inhibitor of anti-apoptotic molecule Bcl2 (39). Recent studies have shown its inhibitory effects on oxidative phosphorylation and it would be interested to see its effects on oxidative phosphorylation dependent TAMS. The present study identified mouse models that will provide invaluable tools to study TAM heterogeneity in the future. Furthermore, the publicly available scRNA seq datasets of T11 and T12 tumors provide a resource for the scientific community to explore TAM heterogeneity in greater detail.

Future studies using these models may help elucidate the mechanisms by which tumors of the same subtype differentially respond to treatment. A higher proportion of treatment-resistant circulating stem cells may explain the failure of CD8+ memory T cells to mount a strong anti-tumor response. Further studies are also required to elucidate the mechanisms that account for the phenotypic switch following the initial recruitment of macrophages to pathways that recruit immunosuppressive neutrophils. A more detailed analysis of the tumors that recur in the primary and metastatic sites is also needed. These preclinical studies will need to be extended to longitudinal studies in patients with new therapeutic combinations that can target potential immunological transitions to better improve long term progression free survival.

Author Contribution

S.S., C.M.P., X.H.F.Z., and J.M.R. conceptualized the study, designed the experiments and wrote the manuscript. S.S. performed the experiments. C.H., S. A., D.P., Y.G., N.Z., and I.B., assisted with the mouse experiments and acquisition of data. L.C., Y.X., and S.L performed IMC staining and analysis. S.S., N.L., I.B., Y.W.W., Y.S., J.S., Z.L., and D.H. analyzed the bioinformatics data and discussed the project direction. J.C., analyzed clinical trial data.

Acknowledgements

We would like to acknowledge Dr. Xi Chen for his help reviewing the manuscript, and Ipshita Thakur for illustrating the mice used in the treatment schemes. We would like to thank Jonathan Shepherd for their help with bioinformatic analysis. These studies were supported by grants NCI-CA148761(C.M.P and J.M.R.), Breast Cancer Research Foundation, NCI CA151293, US Department of Defense DAMD W81XWH-16-1-0073 and W81XWH-18-1-0574, Susan G. Komen CCR14298445, and McNair Medical Institute (X. H.-F. Z.) CPRIT grant RP160283(S.S.), the Dan L. Duncan Comprehensive Cancer Center (NCI: P30: CA125123) and Pathology Core of the Lester and Sue Smith Breast Center. This project also was supported by the Advanced Technology Cores at BCM: Genomic and RNA Profiling Core (NCI: CA125123),

Single Cell Genomics Core, Cytometry and Cell Sorting Core (CPRIT-RP180672), and Integrated Microscopy Core (NIH: DK56338 and CA125123; CPRIT: RP150578 and RP170719).

Declaration of Interests
The authors declare no competing interests.

Main Figure Legends

Figure 1-Low dose chemotherapy is immunostimulatory and combination with a TAM-targeting agent can lead to durable regression in p53-/- murine models of TNBC
a, Heatmap for pathways enriched in p53-/- tumor models. **b,** Cibersort analysis for immune cells on p53 -/- tumor models. **c**, Principal component analysis (PCA) on p53 -/- tumor models d, Single agent CTX treatment led to a reduced tumor burden in Balb/c mice as compared to NSG mice. Data are shown as mean□ S.E.M, n = 10 per group except NSG PBS, n = 5. Multiple unpaired t tests were used to determine significance. **e,** Co-culture of GFP+ T12 tumor cells and GFP targeting T cells with or without Phosphoramide Mustard (PM). Each treatment was performed in triplicates and repeated twice. **f,** Antibody depletion of CD4+ T Cells leads to a significant decrease in response to CTX and increased tumor volumes while differences in response due to depletion of CD8+ T Cells neared statistical significance at day 17, p = 0.06 n = 5-7 mice per group. Multiple unpaired t tests were used to determine significance**. g,** Treatment schema for combination therapy using low-dose Cyclophosphamide (CTX) and a CSF1R inhibitor Pexidartinib (PXB). **h, l, j,** Improved survival in mouse tumor models after combination treatment. Treatment was stopped at day 30. **k,l,m,** Combining low-dose CTX with a Csf1r inhibitor (PXB) lead to a reduction in tumor burden in T12 and 2151R p53-/- mouse tumors and stasis in T11, n = 7-10 mice per group. Survival benefit was assessed by Kaplan-Meier curves using the log-rank (Mantel-Cox) test. Dotted line marks point of treatment cessation.

Figure 2-Imaging Mass Cytometry and Single cell RNA sequencing show that combination treatment can lead to an expansion of CD8+/CD4+ T cells and B cells in responsive T12 tumors. a, Imaging mass cytometry analysis of the tumor immune microenvironment in T12 tumors before and after treatment. Representative images overlaid with 7 markers (F480, Ly6C, Ly6G, CD11b, CD4, CD8a, B220) for each treatment group. **b, c** Map using *t*-distributed stochastic neighbour embedding(*t*-SNE) of immune cells from high dimensional images of T12 tumors from treatment groups-PBS, PXB, CTX, CTX + PXB, n = 3 mice per group. **d, e,** Neighbourhood analysis of T12 tumors in which the color of the squares indicates significant pairwise interactions or avoidance between PhenoGraph defined cellular metaclusters. Highlighted interactions include CD8+/CD4+ T cells (clusters 1-7), B220+ B cells(cluster-14) and CD11C+ CD86+ Dendritic cells (cluster 15). **f,** Schema for the isolation and analysis of single cell RNA/VDJ sequencing. **g,** UMAP plot showing CD45+ immune cell clusters before and after treatment. **h,** UMAP plot showing CD45+ immune cells split by treatment group. **i, j,** Quantification of main immune cell clusters (Feature plots showing the expression levels of murine immune cell marker genes (Cd3e, Cd4, Cd8a, Cd19, Cd68, S100a8, Itgax) in 4 treatment groups.

Figure 3-Combination therapy treated T12 tumors are infiltrated by polyclonally expanded, less differentiated, exhaustion-resistant CD8+ CD127+ memory T cells. a, b, UMAP plot showing CD8+ T Cell clusters of the 4 treatment groups and split by sample type. Clusters were annotated using the Immgen database (1), SingleR(Data not shown) and using known markers. **c,** Quantification of CD8+ T cell subsets in different treatment groups. **d,** Monocle 3 pseudotime plot of CD8+ T cells from all 4 treatment groups in T12 tumors. e, Gene expression of exhaustion and activation/longevity related markers in CD8+ T Cell clusters across pseudotime, split by treatment group. **f, g,** Clonal frequency of CD8+ T cells in all 4 treatment groups and chord diagrams representing unique V-J region pairings in CD8+ T cells in T12 tumors before and after treatment. h, Schema for T12 rechallenge experiments and treatment. **i,** Quantification of mice that completely

or partially (tumor volume < 50 % of control tumors) rejected T12 mammary tumors injected into the contralateral mammary gland of previously treated T12 tumor bearing mice, n = 10.

Figure 4-Tertiary Lymphoid Structures (TLS) infiltrated by antigen experienced CD127+ CD8+/CD4+ memory T cells and antigen presenting B220+ B cells and CD11C+CD86+ Dendritic cells are observed in the tumor beds of long-term responders. a, Imaging Mass Cytometry analysis of TLS observed 30 days post-treatment in long-term responder mice bearing T12 tumors. Representative image overlaid with 4 markers (F480, CD8A, B220, CD4) in combination treated mice. **b,** Quantification of TLS before and after treatment, n = 5-6 mice. Unpaired t-tests were used to obtain significant figures. Mice were collected at different time points due to different end points between treatment groups. c, *t*-SNE projection of cellular metaclusters observed in the TLS. **d, e,** Neighborhood analysis of TLS in the tumor bed of long-term responders where the color of the squares indicates significant pairwise interactions or avoidance between PhenoGraph defined cellular metaclusters as well as quantification of cells per mm^2. Highlighted interactions include CD8+/CD4+ T cells (clusters 1-6), B220+ B cells (cluster 9), CD11C+ Dendritic cells (cluster 10) and avoidance with CD11B+ F480+ TAM clusters (cluster 7). **f, g,** Gene expression feature plots and quantification of CD4+ T cells expressing activating/co-stimulating markers in all 4 treatment groups.

Figure 5-Single cell RNA sequencing and IMC reveal phenotypically similar (CD68+, F480+) but transcriptomically distinct TAMs in responsive(T12) and non-responsive(T11) tumors. a, UMAP plot showing CD68+ Myeloid cells (Monocytes and TAMS) from untreated T12 and T11 tumors**. b,** UMAP plot showing distinct clusters being formed by T12 and T11 CD68+ Myeloid cells with minimal overlap. **c,** Projection of CD68+ Myeloid cells along a pseudotime trajectory with the root point starting at Ly6c2+ monocytes showing that T11 TAMs are less differentiated as compared to T12 TAMs and might follow an aberrant differentiation trajectory. **d,** Plot showing differentially expressed genes between T12 TAMs and T11 TAMs (log2fold change>1.5, $p < 0.05$). **e,** Enrichment of select activation and metabolism related pathways in T12 and T11 CD68+ Myeloid cells using GSEA.

Figure 6- Survival analysis of TNBC patient data a reveal different prognosis for patients with a high T12 or T11 signature before chemotherapy and a higher T11 signature is seen in patients with residual disease (RD) after chemotherapy. a,b,c, Chemotherapy treated TNBC patients with a high T12 vs T11 signature had significantly improved OS as compared to patients with a high T11 vs T12 signature ($p < 0.05$) which showed lower OS for patients across all breast cancer subtypes including TNBC.
d, Analysis of paired TNBC samples before and during NAC reveals an enrichment of the T11vsT12 signature in patients with residual disease and no significant enrichment in patients that undergo pCR.

Figure 7-Combination therapy can be used to treat T12 lung metastasis. a, Treatment schema depicting treatment for mice bearing T12 lung metastasis. **b, c**, Representative images and quantification of metastatic lung nodules in all 4 treatment groups-PBS, PXB, CTX, CTX+PXB, n= 4-5 animals per group, $p < 0.05$).

Supplemental Figure Legends

Supplemental Figure 1-Low dose chemotherapy is immunostimulatory and combination with a TAM targeting agent can lead to durable regression in p53-/- murine models of TNBC a, Treatment response using standard of care drugs on T11 mammary tumors. **b,** Immunohistochemistry for F4/80+ TAMs and CD8+ T Cells on p53-/- tumor models. **c,** T cell gating scheme. **d,** Myeloid cell gating scheme. **e,** Flow cytometry analysis of CD8+ and CD4+ T cells before and after low-dose CTX treatment, n = 6-7 mice per group. **f,** Quantification of TAMs upon antibody depletion of CD4+ T cells after treatment. g, Quantification of CD8+ T cells after CD4+ T cell depletion after treatment. **h,i,** Quantification of CD8+ T memory cell subsets before and after treatment, n = 4-5 mice per group. Unpaired t-test was used to determine significance. **j,** Reduced tumor volume and improved survival in T12 mammary tumor bearing mice after treatment with CTX and 3.3X lower PXB (75 ppm).

Supplemental Figure 2- Imaging Mass Cytometry and Single cell RNA sequencing show that combination treatment can lead to an expansion of CD8+/CD4+ T cells and B cells in responsive T12 tumors. a, Map using *t*-distributed stochastic neighbour embedding(*t*-SNE) of immune cells from high dimensional images of non-responsive T11 tumors from treatment groups-PBS, PXB, CTX, CTX + PXB, n = 3 mice per group. **b,** Neighborhood analysis of T11 tumors in which the color of the squares indicates significant pairwise interactions or avoidance between PhenoGraph defined cellular metaclusters. Highlighted interactions include CD8+/CD4+ T cells (clusters 1-7), B220+ B cells(cluster-15) and CD11C+ CD86+ Dendritic cells (cluster 16). **c,** Quantification of immune cells metaclusters identified in T12 and T11 tumors. Number of cells were obtained per mm^2 and 3 random areas were ablated per tumor section. **d,** Gene expression heatmap for CD45+ immune cells before and after treatment for all treatment groups.

Supplemental Figure 3-Combination therapy treated T12 tumors are infiltrated by polyclonally expanded, less differentiated, exhaustion-resistant CD8+ CD127+ memory T cells. a, Gene expression heatmap for annotated CD8+ T cells before and after treatment in all treatment groups. **b,c,** Feature plots showing the expression of additional memory/exhaustion/activation markers in CD8+ T cells in T12 tumors before and after treatment.

Supplemental Figure 4-Tertiary Lymphoid Structures (TLS) infiltrated by antigen experienced CD8+/CD4+ memory T cells, antigen presenting B220+ B cells and CD11C+CD86+ Dendritic cells are observed in the tumor beds of long-term responders. a, H&E and IHC images of TLS using T cell (CD4+ or CD8+) and B cell (CD19+) markers. **b,** Representative imaging mass cytometry images as well as single channel images depicting the localization of markers of antigen experienced (M2B4+m CD86+) and memory (CD127+) T cells. **c,** Cell density of immune cells in individual clusters in the TLS. **d,** H2-Ab1(MHCII) expression on CD19+ B cells. **e, f,** Chemokine and cytokine analysis from bulk RNA sequencing data for the 3 claudin-low p53-/- tumor models, n = 5-9 mice per tumor model. qPCR for selected cytokines highlighting the significantly higher expression of T cell memory maintenance marker Il7 and IL7R(CD127) in responsive (T12, 2151R) models as compared to non-responsive tumor models(T11).

Supplemental Figure 5-Single cell RNA sequencing and IMC reveal phenotypically similar (CD68+, F480+) but transcriptomically distinct TAMs in responsive(T12) and non-responsive(T11) tumors. a, IMC analysis of T12 and T11 tumors after combination therapy highlighting the spatial localization of CD8+/CD4+ T cells, B cells with respect to proliferating Ki67+ cells and F480+ TAMs. **b,** Quantification of cell density per mm^2 for immune cell types highlighted for T12 and T11 tumors post-treatment. **c,** Feature plots shown monocyte (CD68+, Ly6C2+) and TAM specific (ADGRE1+(F480), CD68+, ARG1+, CSF1R+) marker genes in T12(MRC1+) and T11(S100A4+) CD68+ Myeloid cells. **d,** In-vitro co-culture assay with sorted F480+ TAMs from T12 and T11 tumor models with GFP targeting JEDI T cells and GFP+ T12 tumor cells. Each condition was run in triplicate and the impact of TAMs on T12 tumor cell proliferation was measured by Ki67 staining.

Supplemental Figure 6- Survival analysis of TNBC patient data reveal a different prognosis for patients with a high T12 or T11 signature before chemotherapy and a higher T11 signature is seen in patients with residual disease (RD) after chemotherapy.
a, Chemotherapy treated TNBC patients with a high T12 vs T11 signature had significantly improved OS as compared to patients with a high T11 vs T12 signature ($p < 0.05$) which showed lower OS for patients across all breast cancer subtypes including TNBC.

Methods

Cell Lines

T11 and T12 cell lines were generated in the Rosen laboratory from primary T11 and T12 tumors by selection of epithelial cells expressing the neomycin cassette in G418.and cultured in DMEM/High Glucose with 10 % FBS, 100 IU ml^{-1} penicillin/streptomycin (Lonza), 5 µg/ml insulin, 10 ng/ml mouse EGF, and AA) and hydrocortisone. Cells were maintained in a humidified incubator at 37°C with 5% CO2. Mycoplasma testing was carried out on the cell lines once a month.

Animals Studies
All animals were used according to a protocol approved by the Institutional Animal Care and Use Committee at Baylor College of Medicine. Female 5-6-week-old BALB/c mice were ordered from Envigo Laboratories and experiments were carried out in age matched animals. Female 5-6-week-old NSG mice (NOD.Cg-Prkdc scid il2rg tm1 Wjl/SzJ)(Stock no 005557) were ordered from Jackson Labs.

Mice were house in the TMF Mouse Facility at the Baylor College of Medicine in SPF/climate-controlled conditions with 12-hour day or night cycles. They were supplied with fresh chow and water from an autowater system continuously.

Mammary fat pad injection
The generation of T12, T11 and 2151R tumor models has been described and characterized previously(1) and tumor chunks were stored in liquid nitrogen for long-term storage in FBS + 10% DMSO. Prior to surgery, tumor chunks were thawed and washed in PBS. Tumor chunks were implanted directly into a small cavity in the mammary fat pad. Mice were monitored for tumor growth and were randomized into treatment groups when the tumors were approximately 5 mm in diameter.

In-vivo treatment Studies
Cyclophosphamide (Sigma Aldrich, PHR1404-1G) was resuspended in sterile PBS(Lonza) and injected i.p at the concentration of 100 mg/kg, once a week for the entire treatment period and the control mice were injected with the same volume of sterile PBS.
PLX3397 was obtained from Plexxikon, Daichii Sankyo and was added to a chow made by Research Diets. Mice were fed the chow ad libitum. The drug concentration in the chow was 275 ppm in most of the experiments described which corresponds to 5 mg/kg per mouse except for the low-dose experiments with a concentration of 75 ppm. Control mice were given the same chow without PLX3397. Mice were weighed and monitored for signs of drug toxicity weekly. Tumors were measured using calipers 3 times a week for the duration of the treatment.

In-vivo T cell depletion studies
Mice were injected i.p. with anti CD4(100 ug, BE0003-1) or anti CD8(150 ug, BE0061) antibodies obtained from Bioxcell Laboratories, twice times weekly. Optimal antibody concentrations were obtained from previous validation experiments. This was repeated during the entire treatment course.

Tail vein injection
Female 5-7-week-old BALB/c mice were injected with tumor cells dissociated from fresh T12 mammary tumors. Cells (200,000) in sterile PBS were injected in per mouse using a 27-gauge syringe. Mice were randomized into treatment groups at day 10 post injection and were given 3 weekly treatments of CTX and PLX3397 chow ad libitum, following which the mice were sacrificed and the lungs were collected for further analysis.

T cell isolation and In-vitro immunosuppression assay
Spleens were harvested from 8-week-old JEDI mice and physically dissociated using a scalpel. Splenocytes were filtered through a 70-□m cell strainer. Red blood cells were lysed using RBC lysis buffer (#B4300062518TN, Tonbo Biosciences). CD3+ T cells were enriched using negative selection of biotinylated antibodies B220, CD11b, CD11c, and Gr-1 (#559971, BD Pharmingen) and magnetically sorting using EasySep Mouse Biotin Positive Selection kit (#18559, Stemcell). CD3+ T cells were activated using a 1:1 ratio Dynabead Mouse T Activator CD3/CD28 (#00775477, Thermo Scientific) for 72 hrs in T cell media containing RPMI 1640 (VWR), 5% heat inactivated FBS, 55□m ß-mercaptoethanol, and 5ng/ml IL-2(# 202-IL-050/CF, R&D Systems). Activated CD3+ T cells were isolated from Dynabead Mouse T Activator CD3/CD28 (#00775477, Thermo Fisher) using negative selection. T12 unlabeled and GFP labeled cell lines were seeded at a density of 2500 cells per well in a 96-well plate. After 24 hrs, T cells were added at a 10:1 effector/target ratio with 10,000; 1,000; 100; 10; 1; 0□m of phosphoramide mustard (#M123069, MuseChem). Each condition was run in triplicate. The conditions include co-culturing with T cells and drug, and wells with drug alone. The

plate was incubated in an Incucyte (Essen) and fluorescence and phase images were taken every hour for 48 hrs. The analysis was run using Incucyte S3 software and graphed using Graphpad Prism 8.

For co-culture experiments with tumor associated macrophages, TAMS were isolated from fresh T12 or T11 tumors using the marker F480 by FACS sorting. They were seeded at a 1:1 ratio with the T cells in the media mentioned above with 20 % tumor cell conditioned medium. The cells were kept in culture for 72 hours following which the T cells and tumor cells were separated and analyzed by flow.

Tissue staining

Primary tumor and lung tissue were fixed in 4% paraformaldehyde overnight and transferred to 70% ethanol for long-term storage. The tissue was embedded in paraffin blocks by the Breast Center Pathology Core at Baylor College of Medicine. IHC was performed according to Rosen Lab protocols (https://www.bcm.edu/research/labs/jeffrey-rosen/protocols).
Primary antibodies used were ordered from Abcam-anti-CD4(EPR19514), Anti-CD8a (YTS169.4), S100A8(EPR3554), F480(Cl: A3-1) or eBioscience B220(RA3-6B2). Biotinylated secondary antibodies were ordered from Biolegend.

Flow Cytometry

Tumors were dissociated using the MACs mouse tumor dissociation kit(Miltenyl Biotec) and suspended in PBS+1% FBS. The cells were incubated in blocking buffer containing 1:200 CD16/32(clone 93, eBioscience) for 30 min on ice. They were subsequently stained by fluorescent-conjugated primary antibodies at previously validated concentrations for 1 hr on ice. Following three PBS+1 % FBS washes, the cells were resuspended in ice cold PBS or fixed in 1 % PFA for immediate acquisition on the LSR Fortessa at the Baylor College of Medicine FACS and Cell Sorting core. Data was further analyzed using FlowJo Software version 10.0.

The following antibodies against mouse antigens were used: anti-CD3ε (145-2C11), anti-CD4 (GK1.5), anti-CD8 (53-6.7) (all from eBioscience); anti-B220 (RA3-6B2), anti-CD11b (M1/70)), anti-CD45 (30-F11), anti-F4/80 (BM8), anti-Ly6G(IA8)(all from Tonbo); anti-CD127 (SB/199, BD Biosciences), anti-CD44 (IM7, BD Biosciences), anti-CD62L (MEL14, Biolegend), Anti-KI67(16A8, Biolegend), anti-CSF1R(AFS98, Biolegend), anti-KLRG1(2F1, Biolegend).

IMC Staining and Quantification

IMC staining and data processing was done at the Houston Methodist Immuno- Monitoring Core. Metal conjugated antibodies were ordered from Fluidigm or validated and conjugated to metals using the MaxPar antibody conjugation kit (Fluidigm). The antibodies used were suspended in BSA and azide free buffers and after conjugation they were diluted in Candor PBS Antibody Stabilization solution (Candor Bioscience) for longterm storage at 4°C.The antibodies used and metal conjugates are listed in Supplementary Excel File 2.

Paraffin embedded tumor tissue samples were sectioned onto slides with each section having a thickness of 5 um. The sections were baked at 60ºC overnight, deparaffinization was performed in xylene and the sections were rehydrated in a graded series of ethanol solutions (90%, 80%, 70% and 50% for 10 min each. Antigen retrieval was performed using 1 µM sodium citrate buffer (pH 6) for 20 min in a heated water bath. Blocking buffer containing 3% bovine serum albumin in tris-buffered saline (TBS) was added to each section and the slides were incubated at R.T for 1 hr. The sections then were incubated in metal conjugated primary antibodies at 4ºC overnight. The next day, samples were washed 4 times in TBS-T following which they were stained with Cell-ID Intercalator (Fluidigm) for nuclear staining. Three random sections per tumor section measuring 0.5 X 0.5 mm were ablated and imaging mass cytometry data were segmented by ilastik and CellProfiler. Histology topography cytometry analysis toolbox (HistoCAT) and R (Version 1.2.5042) were used to analyze the images and perform clustering and neighborhood analysis.

qPCR Protocol and primer sequences

RNA was isolated from primary mouse tumor tissue using TRIzol reagent (# 15596018, Thermo Scientific). Total RNA was then reversed transcribed into cDNA using the RT2 first-strand kit (#330401, Qiagen). Realtime quantitative RT-PCR was carried out in triplicates utilizing the amfiSure qGreen Q-PCR Master Mix (#Q5602-

005, GenDEPOT) using a StepOnePlus real-time PCR system (Applied Biosystems, Foster City, CA, USA) and analyzed using the comparative Ct method (2−ΔΔCt) with GAPDH as the housekeeping reference gene. The primers utilized are listed in the table below.

GENE NAME	SEQUENCE
EPGN-F	CCATTTGCAGATGCTTTACTGGT
EPGN-R	GCCAATCCCAATCGCAATGTATT
IL12B-F	ATGGAGTCATAGGCTCTGGAAA
IL12B-R	CCGGAGTAATTTGGTGCTTCAC
IL7-F	TTCCTCCACTGATCCTTGTTCT
IL7-R	AGCAGCTTCCTTTGTATCATCAC
IL7R-F	GCGGACGATCACTCCTTCTG
IL7R-R	AGCCCCACATATTTGAAATTCCA
CCL4-F	TTCCTGCTGTTTCTCTTACACCT
CCL4-R	CTGTCTGCCTCTTTTGGTCAG
CCR10-F	GGACTTTACTCCGGGTACGAT
CCR10-R	CAGGGAGACACTGGGTTGGA
CXCL1-F	CTGGGATTCACCTCAAGAACATC
CXCL1-R	CAGGGTCAAGGCAAGCCTC
LIF-F	ATTGTGCCCTTACTGCTGCTG
LIF-R	GCCAGTTGATTCTTGATCTGGT
IL11-F	TGTTCTCCTAACCCGATCCCT
IL11-R	CAGGAAGCTGCAAAGATCCCA
NPPB-F	GAGGTCACTCCTATCCTCTGG
NPPB-R	GCCATTTCCTCCGACTTTTCTC
TNFRSF-F	CAGGCCCCTACAGACAACAC
TNFRSF-R	ACTCGTCTCCCACAAGGAACT
SLIT2-F	CCATGTAAAAATGATGGCACCTG
SLIT2-R	ATCACAGTCCTGACCCTTGAA
GAPDH-F	GAGTCAACGGATTTGGTCGT
GAPDH-R	GACAAGCTTCCCGTTCTCAG

RNA sequencing analysis

Tumor sample mRNA quality was measured using the Agilent Bioanalyzer and libraries for mRNA-seq were made using total RNA and the Illumina TruSeq mRNA sample preparation kit. Paired end (2x50bp) sequencing was performed on a Illumina HiSeq 2000/2500 sequencer at the UNC High Throughput Sequencing Facility.

Consequential fastq files were aligned to the mouse mm10 reference genome using the STAR aligner algorithm (40). Ensuing BAM files were sorted and indexed using Samtools and quality control was performed using Picard. Transcript read counts were determined was performed using Salmon(41). The RNA-seq data was processed and normalized as published (2). Gene expression signatures were calculated as the median expression of all the genes in the signature as published(42). Non treated tumors from existing published gene expression data were used for this study (Hollern et al. 2019) and can be accessed on the Gene Expression Omnibus (GEO) under accession GSE124821.

Single cell isolation and scRNA sequencing analysis

Tumors were dissociated as described previously and CD45+ cells were isolated from tumors using the Miltenyi Magnetic Enrichment Kit or FACS sorting. Fresh cells were suspended in PBS and library preparation was carried out by the Single Cell RNA Sequencing core at Baylor College of Medicine using the 10X Genomics Chromium RNA seq 5 prime Kit. The samples were sequenced at the Genomic and RNA Profiling Core at Baylor College of Medicine on Nextseq 500 or NovaSeq 6000 sequencing machines from Illumina. Raw data has been uploaded on GEO under accession number GSE165987.

Cellranger Count and vdj

Fastq files with range of 26-28bps for R1 and 89-96bps for R2 were processed using the Cell Ranger Single Cell Software Suite provided by 10x Genomics, V3.0.2. Reads were aligned to mouse genome (mm10) which is available on Cellranger's website http://cf.10xgenomics.com/supp/cell-exp/refdata-cellranger-mm103.0.0.tar.gz. Filtered gene-barcodes matrices that passes the default Cellranger threshold for detection were used for further analysis. We obtained an average of 1803 unique genes per cell with a median of 1413 and an average of 7668 unique transcripts per cell with a median of 4147 which is comparable to similar scRNASeq studies. For the VDJ samples, the fastq files were processed using the Cellranger vdj pipeline and the reads were aligned to the GRCm38 reference genome which is also available on Cellranger's website at http://cf.10xgenomics.com/supp/cell-vdj/refdata-cellranger-vdj-GRCm38alts-ensembl-2.2.0.tar.gz.

Data Processing

The first analysis which studies T cells consisted of four samples: 16805(PBS), 17746(CSF1R), JR20876(Combination) and JR20877(CTX). The second analysis studying myeloid cells consisted of four samples: T12(16800 and 16805) and T11(Gao1 and Gao2) mice models. All downstream analyses were performed using Seurat R package, V3.1.3 and Monocle3_0.2.0.

Seurat

Downstream analysis of the RNA data was performed using the Seurat R package, V3.1.3 (43). Cells with greater than 10% mitochondria expression were removed. Outlier cells with greater than 40,000 were removed. All rps, rpl, mt and gm genes were also removed. The data were normalized and the top 3000 genes with the highest residual variance were selected as the highly variable genes Seurat's SCTransform. SCTransform also filters out genes that are present in less than 5 cells. This resulted in 31167 cells and 15976 genes from 36198 cells and 31053 genes for the T Cell study and 19352 cells and 15365 genes from 21325 cells and 31053 genes for the Myeloid study. The PCA scores were computed using Seurat's RunPCA function and the clusters were identified using first 30PCs with a resolution of 1.2 for the T Cell study while the Myeloid study uses the same number of PCs but with a resolution of 0.8. The UMAP projection were for both studies were generated using the first 30PCs with a default parameter of 0.3 minimum distance and k = 30 neighbors.

The T Cell study samples were further split into CD4 T cells and CD8 T cells. CD4 T cells were subset based on Cd4 > 0.5 and Cd3e >1 while CD8 T cells were subset based on Cd8a > 0.5 and Cd3e > 1. Cells that intersect between the CD4 and CD8 T cells subset were removed. This resulted in a subset of 3859 unique CD4 T cells and 2346 unique CD8 T c ells and the raw counts with the original number of genes of 23393(rps, rpl, mt and gm genes were removed). SCTransform was performed on both the CD4 and CD8 T cell subset which resulted in 3859 cells and 11758 genes and 2346 cells and 11918 genes for CD8 T cell. For

CD4 T cells, the PCA scores were recalculated and the clusters were reidentified using the first 30PCs with a resolution of 1.5. For CD8 T cells, the clusters were identified using the first 50 recalculated PCs resolution of 1.0. The UMAP projection were regenerated using the first 30PCs for CD4 T cells while CD8 T cells used the first 50PCs. The other UMAP parameters remained unchanged with a default parameter of 0.3 minimum distance and k = 30 neighbors.
For the Myeloid study, macrophages and monocytes cells were subset based on the SingleR Immgen annotation that is explained below or expression of CD68 using a threshold of > 0.5. 15718 cells were subset with the raw counts of the original 23393 genes. The data are renormalized using SCTransform which outputs 15718 cells and 14688 genes. The PCA scores were recomputed and 30PCs were used to reidentify the clusters with a resolution of 0.8. The UMAP projection were obtained using the first 30PCs with the default parameter of 0.3 minimum distance and k = 30 neighbors.

Annotation
Clusters of both studies were annotated using the new SingleR, V1.0.5 (44). The IMMGEN reference(53) which has a collection of 830 microarray samples - with 20 main cell types and 253 subtypes – was used as the reference to annotate the dataset. As noted above for the myeloid study, the cells were first annotated using SingleR prior to being subset. For CD8 T cell, the clusters were manually annotated with the following annotation: Nfκbia+ CD8+ Tcm(Cluster 0, 6, 7, 9, 11 and 13), Ly6a CD8+ Tcm (Cluster 2), Smad7+ CD8+ Tn (Cluster 1 and 14), Gzmb+ CD8+ Teff (Cluster 4 and 5), Mki67+ CD8+ Tprof (Cluster 12) and Lag3+ CD8+ Tex(Cluster 3 and 10).

Differentially Expressed Genes
A differential expression test was done using the Wilcoxon Rank Sum test which is the default of Seurat's FindMarkers function for all genes that has not been filtered out. Logfc threshold = 0 and min.pct = 0 parameters were used. The test was conducted for both the Seurat clusters and the cell type clusters annotated by SingleR. Three extra comparison were made for CD4 and CD8 T cells which were combination vs CSF1R, combination vs CTX and combination vs all.

Pseudotime Analysis
The pseudotime trajectory of CD4 and CD8 T cells as well as macrophages/monocytes cells was obtained using the monocle 3 pipeline, V3.0.2 (16). For all three analyses, there was a further subset based on the Seurat clusters or SingleR annotation. We filtered out Monocytes from CD8 T cells, B cells from CD4 T Cells and for the Myeloid study, Cluster 14 and 19 were filtered out due to being outliers. The monocle3 pipeline was customized to utilize the already computed Seurat's UMAP embeddings. The partitions that were determined by Monocle were manually set to one to have a continuous lineage. The branches and leaf point index number were manually modified to show sequence.

VDJ sequencing analysis
TCR reads were mapped to the GRCm38 reference genome using CellRanger vdj (10x Genomics, version 3.0.2) pipeline. In total, 18791 cells are detected with an average 115,188 reads per cell. In total, 92.8% of cells are annotated T cells and 78.9% cells have mapped TRA read while 88.0% cells have mapped TRB reads. The clonotype analysis considers cells with at least one of the TRA and TRB sequence. For the VJ recombination analysis, we found a total of 14140 cells with productive VJ spanning pair VJ pairs. For each sample, we filtered out V gene and J gene low abundance (the abundance is less than 3% per sample) and plotted the chord diagram.

Pathway Analysis
Pathway analysis was carried out on subsets of CD68+ myeloid Cells in T12 and T11 tumors. Differential Gene Expression was obtained using the Wilcoxan Rank Sum Test, logFc > 0.5 using R studio. Signatures obtained were labeled T12vsT11 and T11vsT12 signatures (Excel, Table 3) and they were used for pathway analysis and patient data analysis in the paper. GSEA analysis was used to determine if pathways were statistically different in the tumor models using FDR < 0.1 as cut off (45). Gene signature pathways related to immunity or metabolism were downloaded from MSigDB (46).

Patient Data Analysis
We scored the association between the T12vsT11 and T11vsT12 signatures and outcomes in triple negative breast cancers using RNA-Seq data using a recently published TNBC patient data set (52). The data was preprocessed using the BETSY platform (48) using a STAR aligner (40) and HTSeq-Count to determine read counts (49) or the raw count matrix that was provided. The signatures were scored using ssGSEA (50).Batch effects were assessed using a principal component analysis and were removed using COMBAT (51). Additional survival analysis was done on R using packages survminer and survival.

Statistical methods.
Sample sizes were not predetermined for treatment studies and are denoted in the figure legends. Each in-vivo experiment was repeated at least 3 times with independent cohorts of mice. Data was show as the mean +- the SEM. All in-vitro experiments were repeated 3 times independently. Each condition was done in biological replicates and the combined data was used to determine the P values.

Statistical analysis was carried out using Graphpad Prism or R Studio (Version 1.2.5042). Statistical significance for tumor volumes was carried out using unpaired paired t-tests or two-way ANOVA (Analysis of variance) with the p value lower than 0.05 being considered significant. Survival analyses were evaluated by Kaplan-Meier curves and the log-rank (Mantel-Cox) test.

Methods References

1. Herschkowitz JI, Zhao W, Zhang M, Usary J, Murrow G, Edwards D, Knezevic J, Greene SB, Darr D, Troester MA, Hilsenbeck SG, Medina D, Perou CM, Rosen JM. Comparative oncogenomics identifies breast tumors enriched in functional tumor-initiating cells. Proc Natl Acad Sci U S A. 2012;109(8):2778-83. Epub 2011/06/03. doi: 10.1073/pnas.1018862108. PubMed PMID: 21633010; PMCID: PMC3286979.
2. Dobin A, Davis CA, Schlesinger F, Drenkow J, Zaleski C, Jha S, Batut P, Chaisson M, Gingeras TR. STAR: ultrafast universal RNA-seq aligner. Bioinformatics. 2013;29(1):15-21.
3. Patro R, Duggal G, Kingsford C. Salmon: accurate, versatile and ultrafast quantification from RNA-seq data using lightweight-alignment. bioRxiv. 2015:021592.
4. Hollern DP, Xu N, Thennavan A, Glodowski C, Garcia-Recio S, Mott KR, He X, Garay JP, CareyEwend K, Marron D, Ford J, Liu S, Vick SC, Martin M, Parker JS, Vincent BG, Serody JS, Perou CM. B Cells and T Follicular Helper Cells Mediate Response to Checkpoint Inhibitors in High Mutation Burden Mouse Models of Breast Cancer. Cell. 2019;179(5):1191-206 e21. Epub 2019/11/16. doi: 10.1016/j.cell.2019.10. 028.PubMed PMID: 31730857; PMCID: PMC6911685.
5. Fan C, Prat A, Parker JS, Liu Y, Carey LA, Troester MA, Perou CM. Building prognostic models for breast cancer patients using clinical variables and hundreds of gene expression signatures. BMC medical genomics. 2011;4(1):1.
6. Stuart T, Butler A, Hoffman P, Hafemeister C, Papalexi E, Mauck WM, 3rd, Hao Y, Stoeckius M, Smibert P, Satija R. Comprehensive Integration of Single-Cell Data. Cell. 2019;177(7):1888-902 e21. Epub 2019/06/11. doi: 10.1016/j.cell.2019.05.031. PubMed PMID: 31178118; PMCID: PMC6687398.
7. Aran D, Looney AP, Liu L, Wu E, Fong V, Hsu A, Chak S, Naikawadi RP, Wolters PJ, Abate AR, Butte AJ, Bhattacharya M. Reference-based analysis of lung single-cell sequencing reveals a transitional profibrotic macrophage. Nat Immunol. 2019;20(2):163-72. Epub 2019/01/16. doi: 10.1038/s41590-018-0276-y. PubMed PMID: 30643263; PMCID: PMC6340744.
8. Cao J, Spielmann M, Qiu X, Huang X, Ibrahim DM, Hill AJ, Zhang F, Mundlos S, Christiansen L,Steemers FJ, Trapnell C, Shendure J. The single-cell transcriptional landscape of mammalian organogenesis. Nature. 2019;566(7745):496-502. Epub 2019/02/23. doi: 10.1038/s41586-019-0969-x. PubMed PMID:30787437; PMCID: PMC6434952.
9. Subramanian A, Tamayo P, Mootha VK, Mukherjee S, Ebert BL, Gillette MA, Paulovich A, Pomeroy SL, Golub TR, Lander ES, Mesirov JP. Gene set enrichment analysis: a knowledge-based approach for

interpreting genome-wide expression profiles. Proc Natl Acad Sci U S A. 2005;102(43):15545-50. Epub 2005/10/04. doi: 10.1073/pnas.0506580102. PubMed PMID: 16199517; PMCID: PMC1239896.

10. Liberzon A, Subramanian A, Pinchback R, Thorvaldsdottir H, Tamayo P, Mesirov JP. Molecular signatures database (MSigDB) 3.0. Bioinformatics. 2011;27(12):1739-40. Epub 2011/05/07. doi:10.1093/bioinformatics/btr260. PubMed PMID: 21546393; PMCID: PMC3106198.
11. Seth S, Huo L, Rauch GM, Adrada BE, Piwnica-Worms H, Thompson AM, Mittendorf EA, Litton JK, Symmans WF, Draetta GF, Futreal A, Moulder SL, Chang J. Delineating longitudinal patterns of response to neoadjuvant systemic therapy (NAST) in triple-negative breast cancer (TNBC): Profiling results from a randomized, TNBC enrolling trial to confirm molecular profiling improves survival (ARTEMIS; NCT02276443).Journal of Clinical Oncology. 2019;37(15_suppl):586-. doi: 10.1200/JCO.2019.37.15_suppl.586.
12. Symmans WF, Peintinger F, Hatzis C, Rajan R, Kuerer H, Valero V, Assad L, Poniecka A, Hennessy B, Green M, Buzdar AU, Singletary SE, Hortobagyi GN, Pusztai L. Measurement of residual breast cancer burden to predict survival after neoadjuvant chemotherapy. J Clin Oncol. 2007;25(28):4414-22. Epub 2007/09/06. doi:10.1200/jco.2007.10.6823. PubMed PMID: 17785706.
13. Chen X, Chang JT. Planning bioinformatics workflows using an expert system. Bioinformatics.2017;33(8):1210-5. Epub 2017/01/06. doi: 10.1093/bioinformatics/btw817. PubMed PMID: 28052928; PMCID:PMC5860174.
14. Anders S, Pyl PT, Huber W. HTSeq--a Python framework to work with high-throughput sequencing data. Bioinformatics. 2015;31(2):166-9. Epub 2014/09/28. doi: 10.1093/bioinformatics/btu638. PubMed PMID: 25260700; PMCID: PMC4287950.
15. Hänzelmann S, Castelo R, Guinney J. GSVA: gene set variation analysis for microarray and RNA-seq data. BMC Bioinformatics. 2013;14:7. Epub 2013/01/18. doi: 10.1186/1471-2105-14-7. PubMed PMID:23323831; PMCID: PMC3618321.
16. Johnson WE, Li C, Rabinovic A. Adjusting batch effects in microarray expression data using empirical Bayes methods. Biostatistics. 2007;8(1):118-27. Epub 2006/04/25. doi: 10.1093/biostatistics/kxj037. PubMed PMID: 16632515.

Main Text References

1. Herschkowitz JI, Zhao W, Zhang M, Usary J, Murrow G, Edwards D, Knezevic J, Greene SB, Darr D, Troester MA, Hilsenbeck SG, Medina D, Perou CM, Rosen JM. Comparative oncogenomics identifies breast tumors enriched in functional tumor-initiating cells. Proc Natl Acad Sci U S A. 2012;109(8):2778-83. Epub 2011/06/03. doi: 10.1073/pnas.1018862108. PubMed PMID: 21633010; PMCID: PMC3286979.
2. Hollern DP, Xu N, Thennavan A, Glodowski C, Garcia-Recio S, Mott KR, He X, Garay JP, Carey-Ewend K,Marron D, Ford J, Liu S, Vick SC, Martin M, Parker JS, Vincent BG, Serody JS, Perou CM. B Cells and T Follicular Helper Cells Mediate Response to Checkpoint Inhibitors in High Mutation Burden Mouse Models of Breast Cancer. Cell. 2019;179(5):1191-206 e21. Epub 2019/11/16. doi: 10.1016/j.cell.2019.10.028. PubMed PMID:31730857; PMCID: PMC6911685.
3. Pfefferle AD, Agrawal YN, Koboldt DC, Kanchi KL, Herschkowitz JI, Mardis ER, Rosen JM, Perou CM. Genomic profiling of murine mammary tumors identifies potential personalized drug targets for p53-deficient mammary cancers. Dis Model Mech. 2016;9(7):749-57. Epub 2016/05/07. doi: 10.1242/dmm.025239. PubMed PMID: 27149990; PMCID: PMC4958311.
4. Hollern DP, Contreras CM, Dance-Barnes S, Silva GO, Pfefferle AD, Xiong J, Darr DB, Usary J, Mott KR, Perou CM. A mouse model featuring tissue-specific deletion of p53 and Brca1 gives rise to mammary tumors with genomic and transcriptomic similarities to human basal-like breast cancer. Breast Cancer Res Treat.2019;174(1):143-55. Epub 2018/11/30. doi: 10.1007/s10549-018-5061-y. PubMed PMID: 30484104; PMCID:PMC6418066.
5. Usary J, Zhao W, Darr D, Roberts PJ, Liu M, Balletta L, Karginova O, Jordan J, Combest A, Bridges A, Prat A, Cheang MC, Herschkowitz JI, Rosen JM, Zamboni W, Sharpless NE, Perou CM. Predicting drug responsiveness in human cancers using genetically engineered mice. Clin Cancer Res. 2013;19(17):4889-99. Epub 2013/06/20. doi: 10.1158/1078-0432.CCR-13-0522. PubMed PMID: 23780888; PMCID: PMC3778918.
6. Hollern DP, Contreras CM, Dance-Barnes S, Silva GO, Pfefferle AD, Xiong J, Darr DB, Usary J, Mott KR, Perou CM. A mouse model featuring tissue-specific deletion of p53 and Brca1 gives rise to mammary tumors with genomic and transcriptomic similarities to human basal-like breast cancer. Breast Cancer Res Treat. 2018.Epub 2018/11/30. doi: 10.1007/s10549-018-5061-y. PubMed PMID: 30484104.
7. Pfefferle AD, Herschkowitz JI, Usary J, Harrell JC, Spike BT, Adams JR, Torres-Arzayus MI, Brown M, Egan SE, Wahl GM, Rosen JM, Perou CM. Transcriptomic classification of genetically engineered mouse models of breast cancer identifies human subtype counterparts. Genome Biol. 2013;14(11):R125. Epub 2013/11/14. doi: 10.1186/gb-2013-14-11-r125. PubMed PMID: 24220145; PMCID: PMC4053990.
8. Kim IS, Gao Y, Welte T, Wang H, Liu J, Janghorban M, Sheng K, Niu Y, Goldstein A, Zhao N, Bado I, Lo HC, Toneff MJ, Nguyen T, Bu W, Jiang W, Arnold J, Gu F, He J, Jebakumar D, Walker K, Li Y, Mo Q, Westbrook TF, Zong C, Rao A, Sreekumar A, Rosen JM, Zhang XH. Immuno-subtyping of breast cancer reveals distinct myeloid cell profiles and immunotherapy resistance mechanisms. Nat Cell Biol. 2019;21(9):1113-26. Epub 2019/08/28. doi: 10.1038/s41556-019-0373-7. PubMed PMID: 31451770; PMCID: PMC6726554.
9. Cabrita R, Lauss M, Sanna A, Donia M, Skaarup Larsen M, Mitra S, Johansson I, Phung B, Harbst K,Vallon-Christersson J, van Schoiack A, Lovgren K, Warren S, Jirstrom K, Olsson H, Pietras K, Ingvar C, Isaksson K, Schadendorf D, Schmidt H, Bastholt L, Carneiro A, Wargo JA, Svane IM, Jonsson G. Tertiary lymphoid structures improve immunotherapy and survival in melanoma. Nature. 2020;577(7791):561-5. Epub 2020/01/17. doi:10.1038/s41586-019-1914-8. PubMed PMID: 31942071.
10. Khan KA, Ponce de Leon JL, Benguigui M, Xu P, Chow A, Cruz-Munoz W, Man S, Shaked Y, Kerbel RS. Immunostimulatory and anti-tumor metronomic cyclophosphamide regimens assessed in primary orthotopic and metastatic murine breast cancer. NPJ Breast Cancer. 2020;6:29. Epub 2020/07/25. doi: 10.1038/s41523020-0171-1. PubMed PMID: 32704531; PMCID: PMC7371860.

11. Agudo J, Ruzo A, Park ES, Sweeney R, Kana V, Wu M, Zhao Y, Egli D, Merad M, Brown BD. GFP-specific CD8 T cells enable targeted cell depletion and visualization of T-cell interactions. Nat Biotechnol.2015;33(12):1287-92. Epub 2015/11/03. doi: 10.1038/nbt.3386. PubMed PMID: 26524661; PMCID:PMC4675673.
12. Rojo R, Raper A, Ozdemir DD, Lefevre L, Grabert K, Wollscheid-Lengeling E, Bradford B, Caruso M, Gazova I, Sanchez A, Lisowski ZM, Alves J, Molina-Gonzalez I, Davtyan H, Lodge RJ, Glover JD, Wallace R,Munro DAD, David E, Amit I, Miron VE, Priller J, Jenkins SJ, Hardingham GE, Blurton-Jones M, Mabbott NA, Summers KM, Hohenstein P, Hume DA, Pridans C. Deletion of a Csf1r enhancer selectively impacts CSF1R expression and development of tissue macrophage populations. Nat Commun. 2019;10(1):3215. Epub 2019/07/22. doi: 10.1038/s41467-019-11053-8. PubMed PMID: 31324781; PMCID: PMC6642117.
13. Patwardhan PP, Surriga O, Beckman MJ, de Stanchina E, Dematteo RP, Tap WD, Schwartz GK. Sustained inhibition of receptor tyrosine kinases and macrophage depletion by PLX3397 and rapamycin as a potential new approach for the treatment of MPNSTs. Clin Cancer Res. 2014;20(12):3146-58. Epub 2014/04/11. doi:10.1158/1078-0432.CCR-13-2576. PubMed PMID: 24718867; PMCID: PMC4060793.
14. Giustini N, Bernthal NM, Bukata SV, Singh AS. Tenosynovial giant cell tumor: case report of a patient effectively treated with pexidartinib (PLX3397) and review of the literature. Clin Sarcoma Res. 2018;8:14. Epub 2018/07/14. doi: 10.1186/s13569-018-0101-2. PubMed PMID: 30002809; PMCID: PMC6038319.
15. Gruosso T, Gigoux M, Manem VSK, Bertos N, Zuo D, Perlitch I, Saleh SMI, Zhao H, Souleimanova M,Johnson RM, Monette A, Ramos VM, Hallett MT, Stagg J, Lapointe R, Omeroglu A, Meterissian S, Buisseret L,Van den Eynden G, Salgado R, Guiot MC, Haibe-Kains B, Park M. Spatially distinct tumor immune microenvironments stratify triple-negative breast cancers. J Clin Invest. 2019;129(4):1785-800. Epub 2019/02/13. doi: 10.1172/JCI96313. PubMed PMID: 30753167; PMCID: PMC6436884.
16. Cao J, Spielmann M, Qiu X, Huang X, Ibrahim DM, Hill AJ, Zhang F, Mundlos S, Christiansen L, Steemers FJ, Trapnell C, Shendure J. The single-cell transcriptional landscape of mammalian organogenesis. Nature.2019;566(7745):496-502. Epub 2019/02/23. doi: 10.1038/s41586-019-0969-x. PubMed PMID: 30787437; PMCID: PMC6434952.
17. Yang CY, Best JA, Knell J, Yang E, Sheridan AD, Jesionek AK, Li HS, Rivera RR, Lind KC, D'Cruz LM, Watowich SS, Murre C, Goldrath AW. The transcriptional regulators Id2 and Id3 control the formation of distinct memory CD8+ T cell subsets. Nat Immunol. 2011;12(12):1221-9. Epub 2011/11/08. doi:10.1038/ni.2158. PubMed PMID: 22057289; PMCID: PMC3872000.
18. Lynn RC, Weber EW, Sotillo E, Gennert D, Xu P, Good Z, Anbunathan H, Lattin J, Jones R, Tieu V, Nagaraja S, Granja J, de Bourcy CFA, Majzner R, Satpathy AT, Quake SR, Monje M, Chang HY, Mackall CL. c-Jun overexpression in CAR T cells induces exhaustion resistance. Nature. 2019;576(7786):293-300. Epub 2019/12/06. doi: 10.1038/s41586-019-1805-z. PubMed PMID: 31802004; PMCID: PMC6944329.
19. Wuerzberger-Davis SM, Chen Y, Yang DT, Kearns JD, Bates PW, Lynch C, Ladell NC, Yu M, Podd A, Zeng H, Huang TT, Wen R, Hoffmann A, Wang D, Miyamoto S. Nuclear export of the NF-kappaB inhibitor IkappaBalpha is required for proper B cell and secondary lymphoid tissue formation. Immunity.2011;34(2):188-200. Epub 2011/02/22. doi: 10.1016/j.immuni.2011.01.014. PubMed PMID: 21333553; PMCID:PMC3111750.
20. de la Fuente H, Cruz-Adalia A, Martinez del Hoyo G, Cibrián-Vera D, Bonay P, Pérez-Hernández D,Vázquez J, Navarro P, Gutierrez-Gallego R, Ramirez-Huesca M, Martín P, Sánchez-Madrid F. The Leukocyte Activation Receptor CD69 Controls T Cell Differentiation through Its Interaction with Galectin-1. Molecular and Cellular Biology. 2014;34(13):2479-87. doi: 10.1128/mcb.00348-14.
21. Menares E, Galvez-Cancino F, Caceres-Morgado P, Ghorani E, Lopez E, Diaz X, Saavedra-Almarza J, Figueroa DA, Roa E, Quezada SA, Lladser A. Tissue-resident memory CD8(+) T cells amplify anti-tumor immunity by triggering antigen spreading through dendritic cells. Nat Commun. 2019;10(1):4401. Epub 2019/09/29. doi: 10.1038/s41467-019-12319-x. PubMed PMID: 31562311; PMCID: PMC6765014.

22. Singh S, Zhang XHF, Rosen JM. TIME Is a Great Healer-Targeting Myeloid Cells in the Tumor Immune Microenvironment to Improve Triple-Negative Breast Cancer Outcomes. Cells. 2020;10(1). Epub 2020/12/31. doi: 10.3390/cells10010011. PubMed PMID: 33374595.
23. Yost KE, Satpathy AT, Wells DK, Qi Y, Wang C, Kageyama R, McNamara KL, Granja JM, Sarin KY, Brown RA, Gupta RK, Curtis C, Bucktrout SL, Davis MM, Chang ALS, Chang HY. Clonal replacement of tumor-specific T cells following PD-1 blockade. Nat Med. 2019;25(8):1251-9. Epub 2019/07/31. doi: 10.1038/s41591-019-05223. PubMed PMID: 31359002; PMCID: PMC6689255.
24. Lehmann PV, Forsthuber T, Miller A, Sercarz EE. Spreading of T-cell autoimmunity to cryptic determinants of an autoantigen. Nature. 1992;358(6382):155-7. Epub 1992/07/09. doi: 10.1038/358155a0.PubMed PMID: 1377368.
25. Grewal IS, Flavell RA. The role of CD40 ligand in costimulation and T-cell activation. Immunol Rev.1996;153:85-106. Epub 1996/10/01. doi: 10.1111/j.1600-065x.1996.tb00921.x. PubMed PMID: 9010720.
26. Lee MKS, Al-Sharea A, Shihata WA, Bertuzzo Veiga C, Cooney OD, Fleetwood AJ, Flynn MC, Claeson E, Palmer CS, Lancaster GI, Henstridge DC, Hamilton JA, Murphy AJ. Glycolysis Is Required for LPS-Induced Activation and Adhesion of Human CD14+CD16− Monocytes. Frontiers in Immunology. 2019;10(2054). doi:10.3389/fimmu.2019.02054.
27. Kawalkowska JZ, Hemmerle T, Pretto F, Matasci M, Neri D, Williams RO. Targeted IL-4 therapy synergizes with dexamethasone to induce a state of tolerance by promoting Treg cells and macrophages in mice with arthritis. European Journal of Immunology. 2016;46(5):1246-57. doi: https://doi.org/10.1002/eji.201546221.
28. Moulder SH, K. Candelaria, R. Rauch, G. Precision neoadjuvant therapy (P-NAT): A planned interim analysis of a randomized, TNBC enrolling trial to confirm molecular profiling improves survival (ARTEMIS). J Clin Oncol 36, 2018 2018;

.

29. Seth S, Huo L, Rauch GM, Adrada BE, Piwnica-Worms H, Thompson AM, Mittendorf EA, Litton JK, Symmans WF, Draetta GF, Futreal A, Moulder SL, Chang J. Delineating longitudinal patterns of response to neoadjuvant systemic therapy (NAST) in triple-negative breast cancer (TNBC): Profiling results from a randomized, TNBC enrolling trial to confirm molecular profiling improves survival (ARTEMIS; NCT02276443).Journal of Clinical Oncology. 2019;37(15_suppl):586-. doi: 10.1200/JCO.2019.37.15_suppl.586.
30. Liedtke C, Mazouni C, Hess KR, Andre F, Tordai A, Mejia JA, Symmans WF, Gonzalez-Angulo AM, Hennessy B, Green M, Cristofanilli M, Hortobagyi GN, Pusztai L. Response to neoadjuvant therapy and longterm survival in patients with triple-negative breast cancer. J Clin Oncol. 2008;26(8):1275-81. Epub 2008/02/06. doi: 10.1200/JCO.2007.14.4147. PubMed PMID: 18250347.
31. Yin L, Duan JJ, Bian XW, Yu SC. Triple-negative breast cancer molecular subtyping and treatment progress. Breast Cancer Res. 2020;22(1):61. Epub 2020/06/11. doi: 10.1186/s13058-020-01296-5. PubMed PMID: 32517735; PMCID: PMC7285581.
32. Patsialou A, Wang Y, Pignatelli J, Chen X, Entenberg D, Oktay M, Condeelis JS. Autocrine CSF1R signaling mediates switching between invasion and proliferation downstream of TGFbeta in claudin-low breast tumor cells. Oncogene. 2015;34(21):2721-31. Epub 2014/08/05. doi: 10.1038/onc.2014.226. PubMed PMID:25088194; PMCID: PMC4317382.
33. Piawah S, Hyland C, Umetsu SE, Esserman LJ, Rugo HS, Chien AJ. A case report of vanishing bile duct syndrome after exposure to pexidartinib (PLX3397) and paclitaxel. NPJ Breast Cancer. 2019;5:17. Epub 2019/06/27. doi: 10.1038/s41523-019-0112-z. PubMed PMID: 31240240; PMCID: PMC6570645.
34. Newman LA, Griffith KA, Jatoi I, Simon MS, Crowe JP, Colditz GA. Meta-analysis of survival in African American and white American patients with breast cancer: ethnicity compared with socioeconomic status. J Clin Oncol. 2006;24(9):1342-9. Epub 2006/03/22. doi: 10.1200/JCO.2005.03.3472. PubMed PMID: 16549828.
35. Adams S, Schmid P, Rugo HS, Winer EP, Loirat D, Awada A, Cescon DW, Iwata H, Campone M, Nanda R,Hui R, Curigliano G, Toppmeyer D, O'Shaughnessy J, Loi S, Paluch-Shimon S, Tan AR, Card D, Zhao J, Karantza V,Cortes J. Pembrolizumab monotherapy for previously treated metastatic triple-

negative breast cancer: cohort A of the phase II KEYNOTE-086 study. Ann Oncol. 2019;30(3):397-404. Epub 2018/11/27. doi:10.1093/annonc/mdy517. PubMed PMID: 30475950.
36. Yang M, McKay D, Pollard JW, Lewis CE. Diverse Functions of Macrophages in Different Tumor Microenvironments. Cancer Res. 2018;78(19):5492-503. Epub 2018/09/13. doi: 10.1158/0008-5472.CAN-181367. PubMed PMID: 30206177; PMCID: PMC6171744.
37. Zhang L, Li Z, Skrzypczynska KM, Fang Q, Zhang W, O'Brien SA, He Y, Wang L, Zhang Q, Kim A, Gao R,Orf J, Wang T, Sawant D, Kang J, Bhatt D, Lu D, Li CM, Rapaport AS, Perez K, Ye Y, Wang S, Hu X, Ren X, Ouyang W, Shen Z, Egen JG, Zhang Z, Yu X. Single-Cell Analyses Inform Mechanisms of Myeloid-Targeted Therapies in Colon Cancer. Cell. 2020;181(2):442-59 e29. Epub 2020/04/18. doi: 10.1016/j.cell.2020.03.048. PubMed PMID:32302573.
38. Bonekamp NA, Peter B, Hillen HS, Felser A, Bergbrede T, Choidas A, Horn M, Unger A, Di Lucrezia R,Atanassov I, Li X, Koch U, Menninger S, Boros J, Habenberger P, Giavalisco P, Cramer P, Denzel MS, Nussbaumer P, Klebl B, Falkenberg M, Gustafsson CM, Larsson NG. Small-molecule inhibitors of human mitochondrial DNA transcription. Nature. 2020. Epub 2020/12/18. doi: 10.1038/s41586-020-03048-z. PubMed PMID: 33328633.
39. Jones CL, Stevens BM, Pollyea DA, Culp-Hill R, Reisz JA, Nemkov T, Gehrke S, Gamboni F, Krug A,Winters A, Pei S, Gustafson A, Ye H, Inguva A, Amaya M, Minhajuddin M, Abbott D, Becker MW, DeGregori J, Smith CA, D'Alessandro A, Jordan CT. Nicotinamide Metabolism Mediates Resistance to Venetoclax in Relapsed Acute Myeloid Leukemia Stem Cells. Cell Stem Cell. 2020;27(5):748-64 e4. Epub 2020/08/22. doi:10.1016/j.stem.2020.07.021. PubMed PMID: 32822582; PMCID: PMC7655603.
40. Dobin A, Davis CA, Schlesinger F, Drenkow J, Zaleski C, Jha S, Batut P, Chaisson M, Gingeras TR. STAR:ultrafast universal RNA-seq aligner. Bioinformatics. 2013;29(1):15-21. Epub 2012/10/30. doi:10.1093/bioinformatics/bts635. PubMed PMID: 23104886; PMCID: PMC3530905.
41. Patro R, Duggal G, Kingsford C. Salmon: accurate, versatile and ultrafast quantification from RNA-seq data using lightweight-alignment. bioRxiv. 2015:021592.
42. Fan C, Prat A, Parker JS, Liu Y, Carey LA, Troester MA, Perou CM. Building prognostic models for breast cancer patients using clinical variables and hundreds of gene expression signatures. BMC medical genomics.2011;4(1):1.
43. Stuart T, Butler A, Hoffman P, Hafemeister C, Papalexi E, Mauck WM, 3rd, Hao Y, Stoeckius M, Smibert P, Satija R. Comprehensive Integration of Single-Cell Data. Cell. 2019;177(7):1888-902 e21. Epub 2019/06/11. doi: 10.1016/j.cell.2019.05.031. PubMed PMID: 31178118; PMCID: PMC6687398.
44. Aran D, Looney AP, Liu L, Wu E, Fong V, Hsu A, Chak S, Naikawadi RP, Wolters PJ, Abate AR, Butte AJ, Bhattacharya M. Reference-based analysis of lung single-cell sequencing reveals a transitional profibrotic macrophage. Nat Immunol. 2019;20(2):163-72. Epub 2019/01/16. doi: 10.1038/s41590-018-0276-y. PubMed PMID: 30643263; PMCID: PMC6340744.
45. Subramanian A, Tamayo P, Mootha VK, Mukherjee S, Ebert BL, Gillette MA, Paulovich A, Pomeroy SL, Golub TR, Lander ES, Mesirov JP. Gene set enrichment analysis: a knowledge-based approach for interpreting genome-wide expression profiles. Proc Natl Acad Sci U S A. 2005;102(43):15545-50. Epub 2005/10/04. doi:10.1073/pnas.0506580102. PubMed PMID: 16199517; PMCID: PMC1239896.
46. Liberzon A, Subramanian A, Pinchback R, Thorvaldsdottir H, Tamayo P, Mesirov JP. Molecular signatures database (MSigDB) 3.0. Bioinformatics. 2011;27(12):1739-40. Epub 2011/05/07. doi:10.1093/bioinformatics/btr260. PubMed PMID: 21546393; PMCID: PMC3106198.
47. Symmans WF, Peintinger F, Hatzis C, Rajan R, Kuerer H, Valero V, Assad L, Poniecka A, Hennessy B, Green M, Buzdar AU, Singletary SE, Hortobagyi GN, Pusztai L. Measurement of residual breast cancer burden to predict survival after neoadjuvant chemotherapy. J Clin Oncol. 2007;25(28):4414-22. Epub 2007/09/06. doi:10.1200/jco.2007.10.6823. PubMed PMID: 17785706.
48. Chen X, Chang JT. Planning bioinformatics workflows using an expert system. Bioinformatics.2017;33(8):1210-5. Epub 2017/01/06. doi: 10.1093/bioinformatics/btw817. PubMed PMID: 28052928; PMCID: PMC5860174.
49. Anders S, Pyl PT, Huber W. HTSeq--a Python framework to work with high-throughput sequencing data. Bioinformatics. 2015;31(2):166-9. Epub 2014/09/28. doi: 10.1093/bioinformatics/btu638. PubMed PMID:25260700; PMCID: PMC4287950.

50. Hänzelmann S, Castelo R, Guinney J. GSVA: gene set variation analysis for microarray and RNA-seq data. BMC Bioinformatics. 2013;14:7. Epub 2013/01/18. doi: 10.1186/1471-2105-14-7. PubMed PMID:23323831; PMCID: PMC3618321.
51. Johnson WE, Li C, Rabinovic A. Adjusting batch effects in microarray expression data using empirical Bayes methods. Biostatistics. 2007;8(1):118-27. Epub 2006/04/25. doi: 10.1093/biostatistics/kxj037. PubMed PMID: 16632515.
52. Park YH, Lal S, Lee JE, Choi YL, Wen J, Ram S, Ding Y, Lee SH, Powell E, Lee SK, Yu JH, Ching KA, Nam JY, Kim SW, Nam SJ, Kim JY, Cho SY, Park S, Kim J, Hwang S, Kim YJ, Bonato V, Fernandez D, Deng S, Wang S, Shin H, Kang ES, Park WY, Rejto PA, Bienkowska J, Kan Z. Chemotherapy induces dynamic immune responses in breast cancers that impact treatment outcome. Nat Commun. 2020;11(1):6175. Epub 2020/12/04. doi: 10.1038/s41467-020-19933-0. PubMed PMID: 33268821; PMCID: PMC7710739.
53. Heng TS, Painter MW, Immunological Genome Project C. The Immunological Genome Project networks of gene expression in immune cells. Nat Immunol. 2008;9(10):1091-4. Epub 2008/09/19. doi: 10.1038/ni1008-1091. PubMed PMID: 18800157.

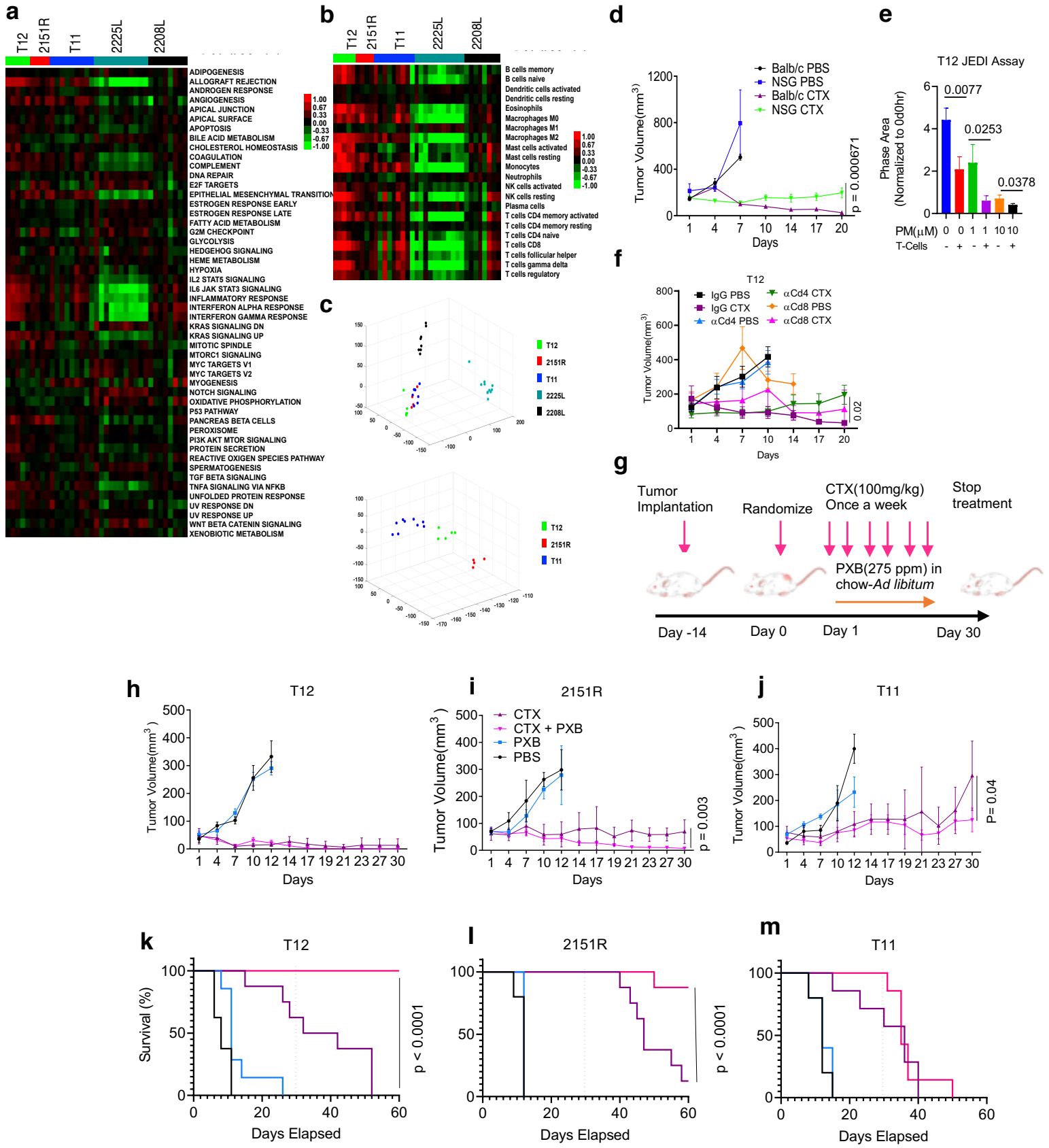

Figure 1, Singh et al.

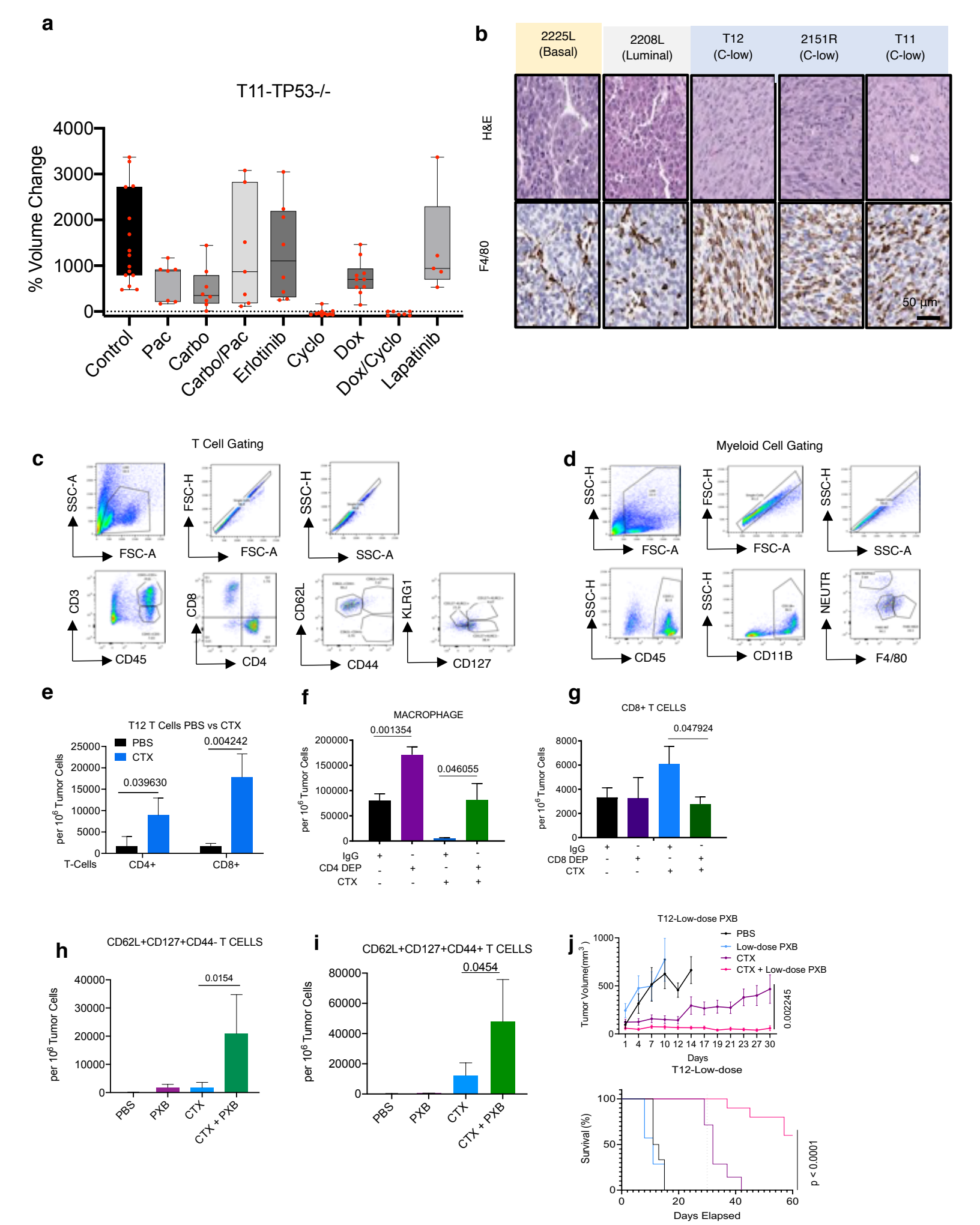

Supplementary Figure 1 for Figure 1, Singh et al.

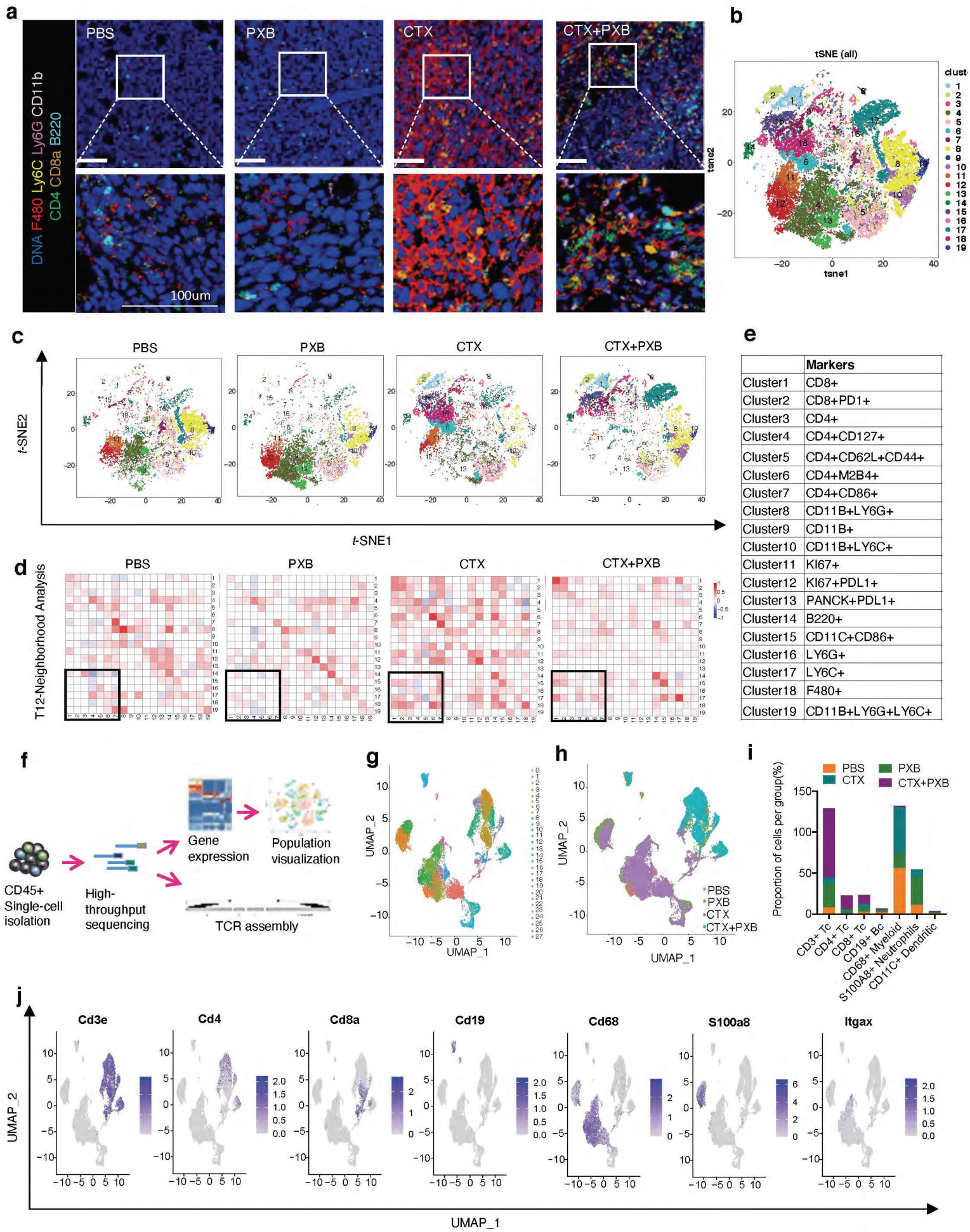

	Markers
Cluster1	CD8+
Cluster2	CD8+PD1+
Cluster3	CD4+
Cluster4	CD4+CD127+
Cluster5	CD4+CD62L+CD44+
Cluster6	CD4+M2B4+
Cluster7	CD4+CD86+
Cluster8	CD11B+LY6G+
Cluster9	CD11B+
Cluster10	CD11B+LY6C+
Cluster11	KI67+
Cluster12	KI67+PDL1+
Cluster13	PANCK+PDL1+
Cluster14	B220+
Cluster15	CD11C+CD86+
Cluster16	LY6G+
Cluster17	LY6C+
Cluster18	F480+
Cluster19	CD11B+LY6G+LY6C+

Figure 2, Singh et al.

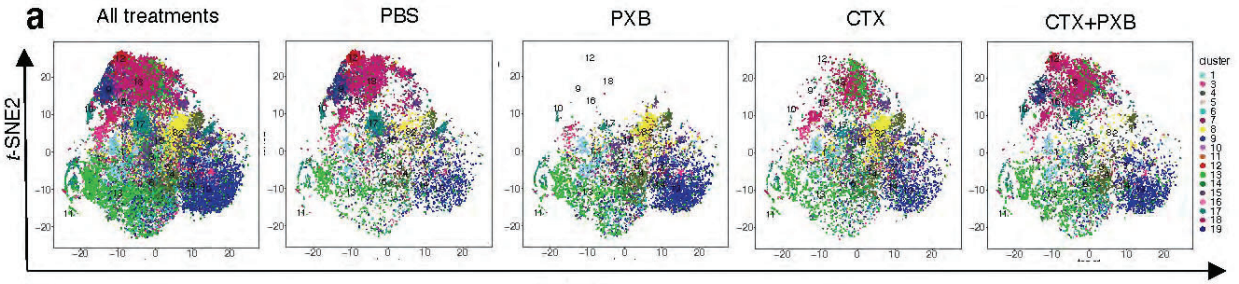

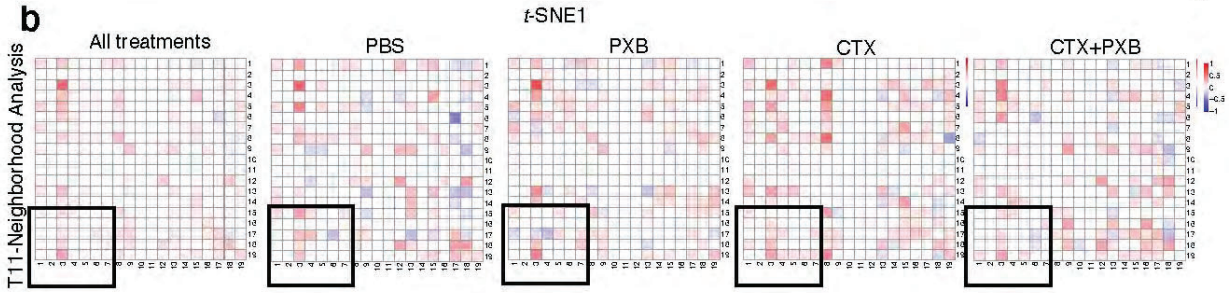

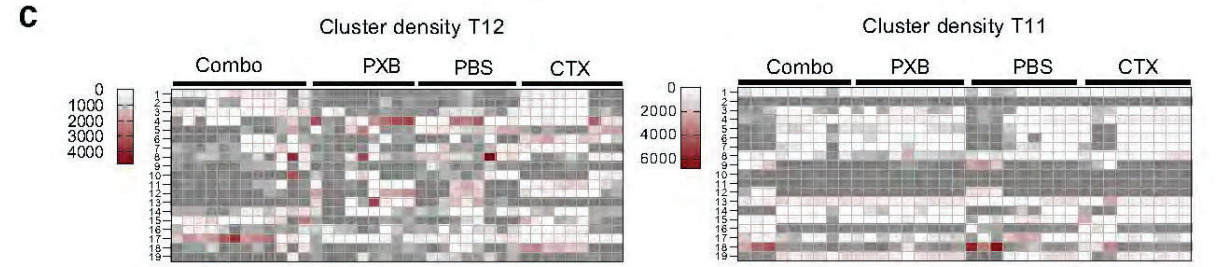

Cluster1	CD8+
Cluster2	CD8+PD1+
Cluster3	CD8+CD127+
Cluster4	CD4+
Cluster5	CD4+PD1+
Cluster6	CD4+CD127+
Cluster7	CD4+CD62L+CD44+
Cluster8	CD4+Foxp3+PD1+
Cluster9	CD11B+F480+
Cluster10	CD11B+LY6G+
Cluster11	CD11B+
Cluster12	KI67+
Cluster13	PANCK+
Cluster14	PANCK+PDL1+
Cluster15	B220+
Cluster16	CD11C+CD86+
Cluster17	LY6G+
Cluster18	LY6C+
Cluster19	LY6G+PDL1+

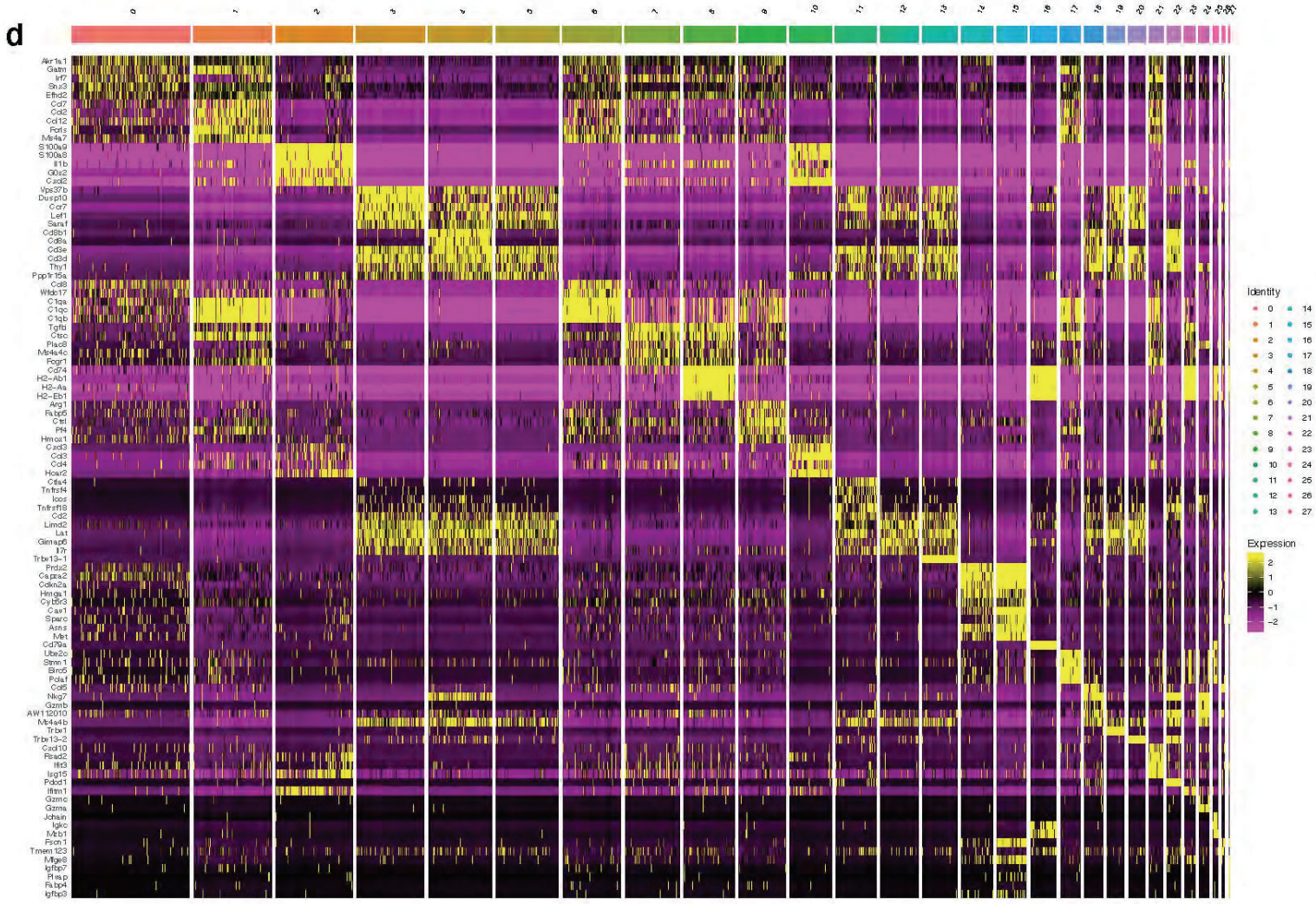

Supplementary Figure 2 for Figure 2, Singh et al.

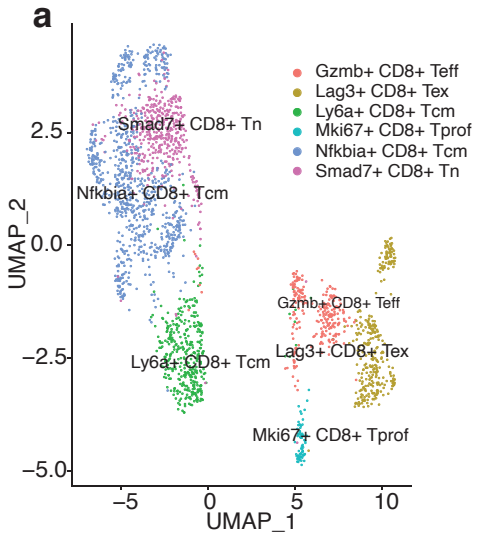

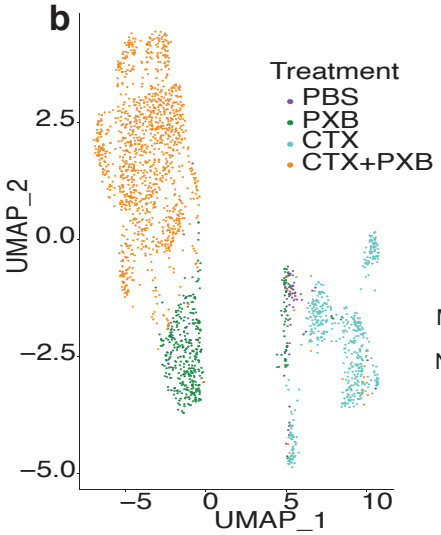

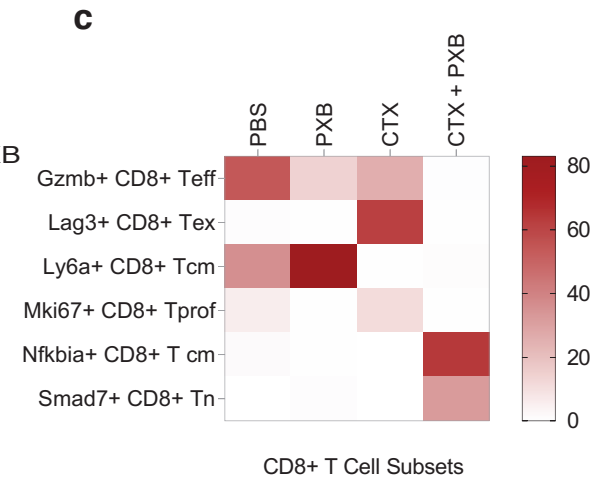

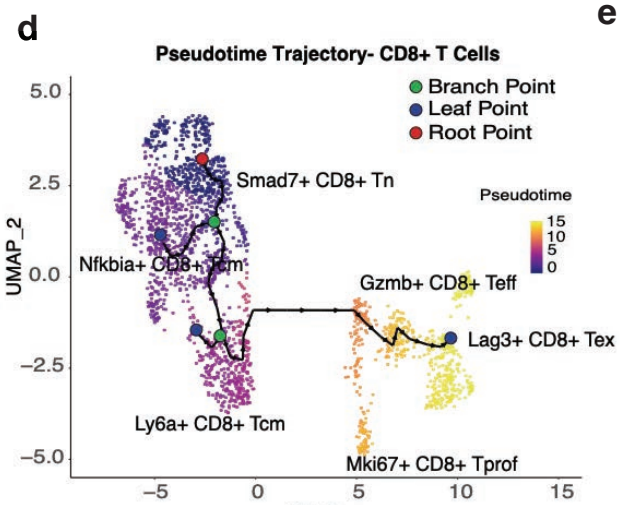

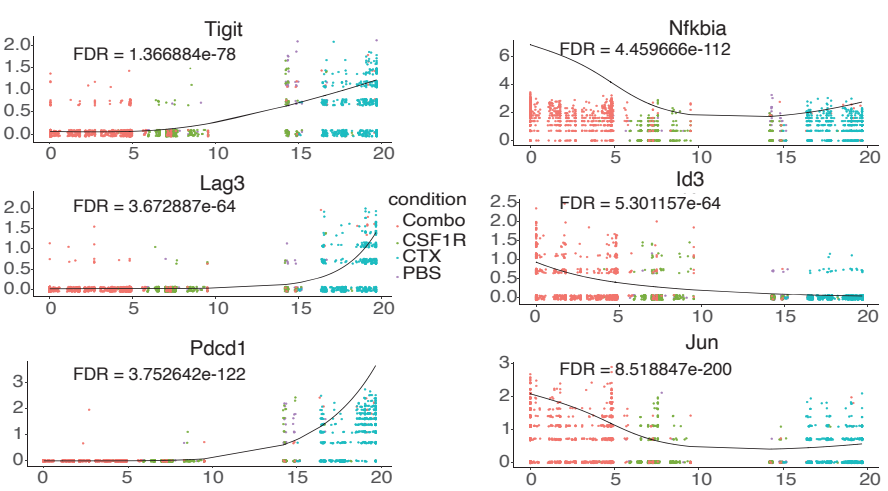

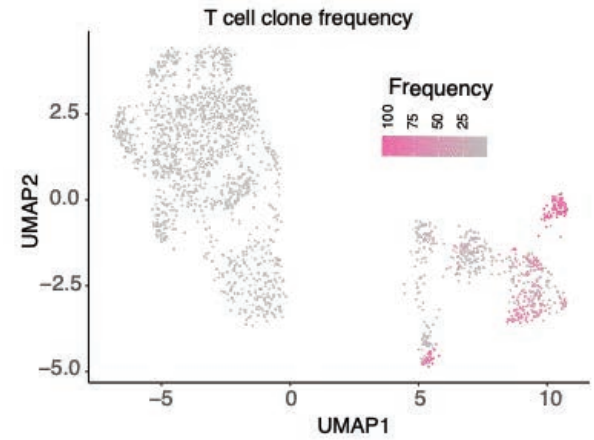

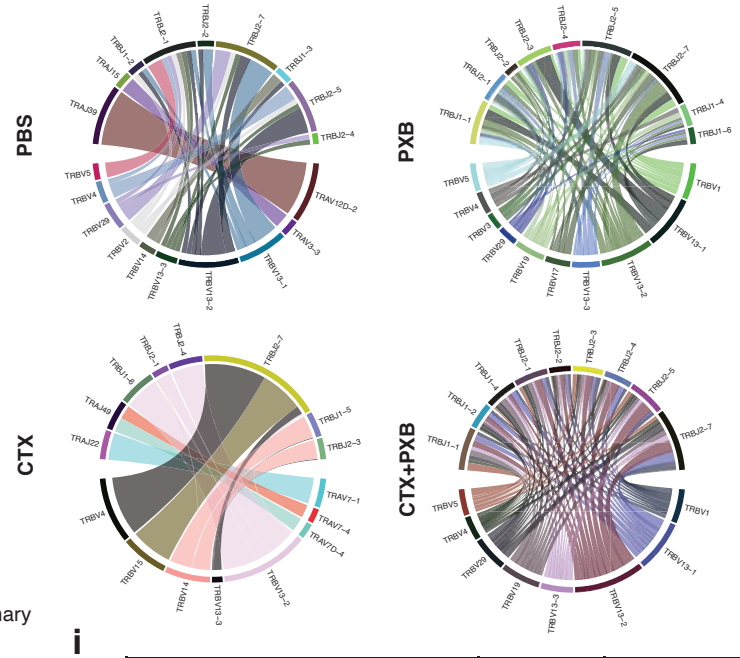

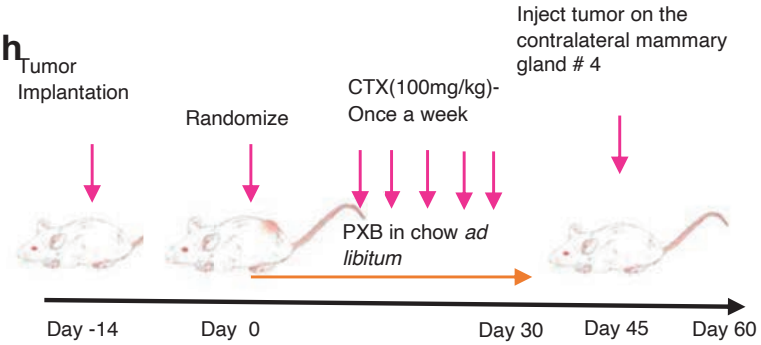

i

Anti-CSF1R + CTX	# of mice	Percentage (%)
Complete rejection	4	40%
Partial rejection (50% tumor volume of NR)	3	30%
No rejection (comparable to control mice	3	30%

Figure 3 Singh et al.

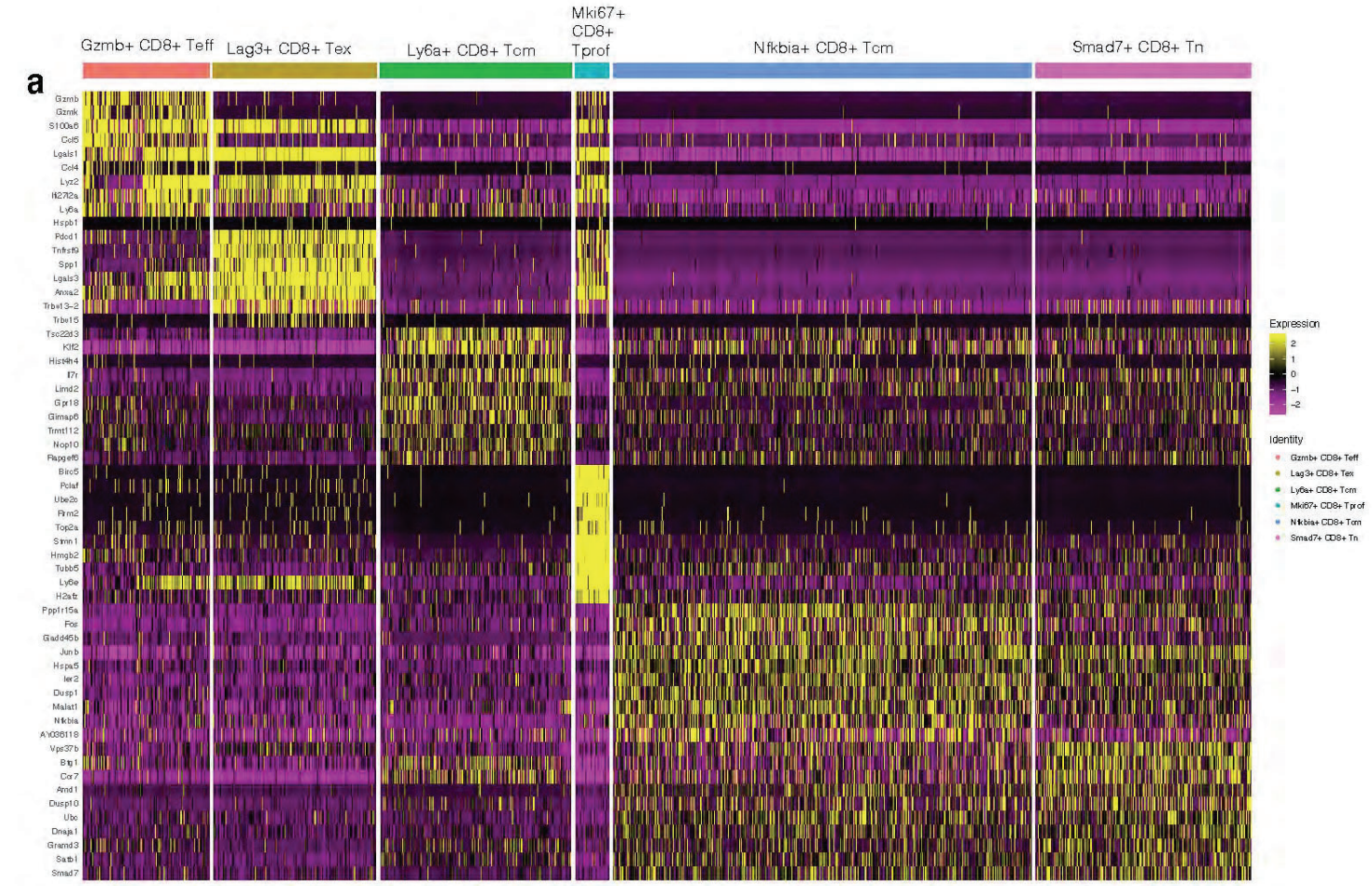

Supplementary Figure 3 for Figure 3, Singh et al.

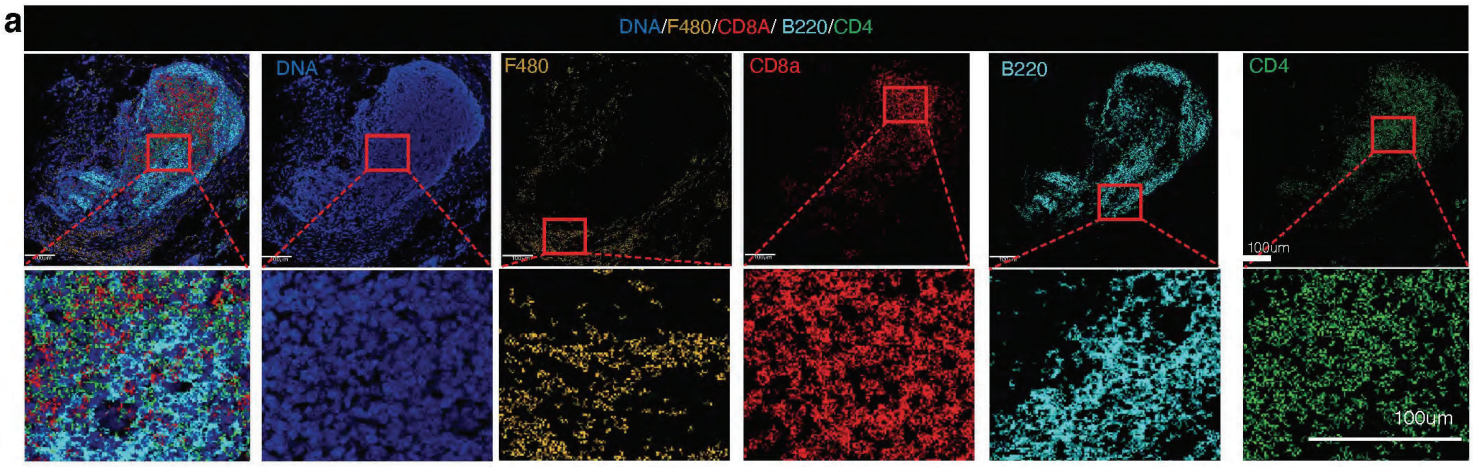

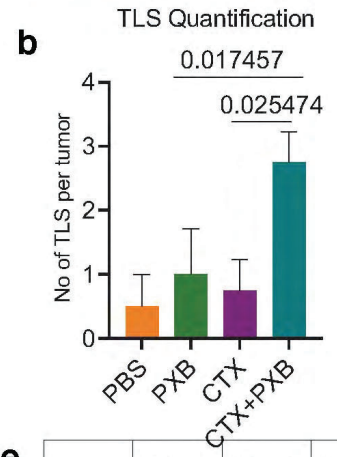

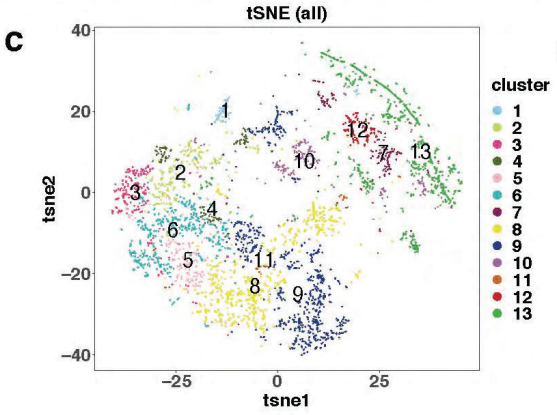

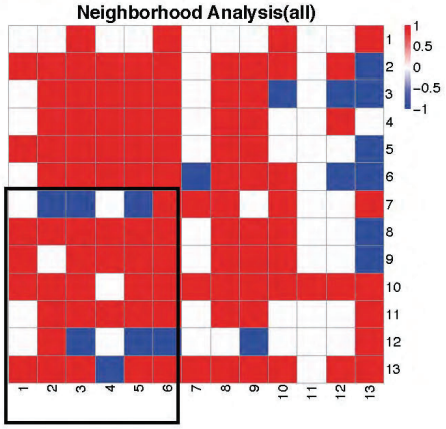

e

	Cluster 1	Cluster 2	Cluster 3	Cluster 4	Cluster 5	Cluster 6	Cluster 7	Cluster 8	Cluster 9	Cluster 10	Cluster 11	Cluster 12	Cluster 13	Cluster 14	Cluster 15
Markers	CD8+	CD8+ CD44+	CD8+ CD86+ CD127+	CD4+ CD44+	CD4+ CD44+	CD4+ CD86+ CD127+	CD11B+ F480+	PANCK+	B220+	CD11C+	LY6G+	LY6C+	F480+	Others	Surface-
Density	156.1905	485.7143	413.3333	257.1429	396.1905	881.9048	281.9048	1253.333	1466.667	426.6667	68.57143	270.4762	1521.905	2100.952	676.1905

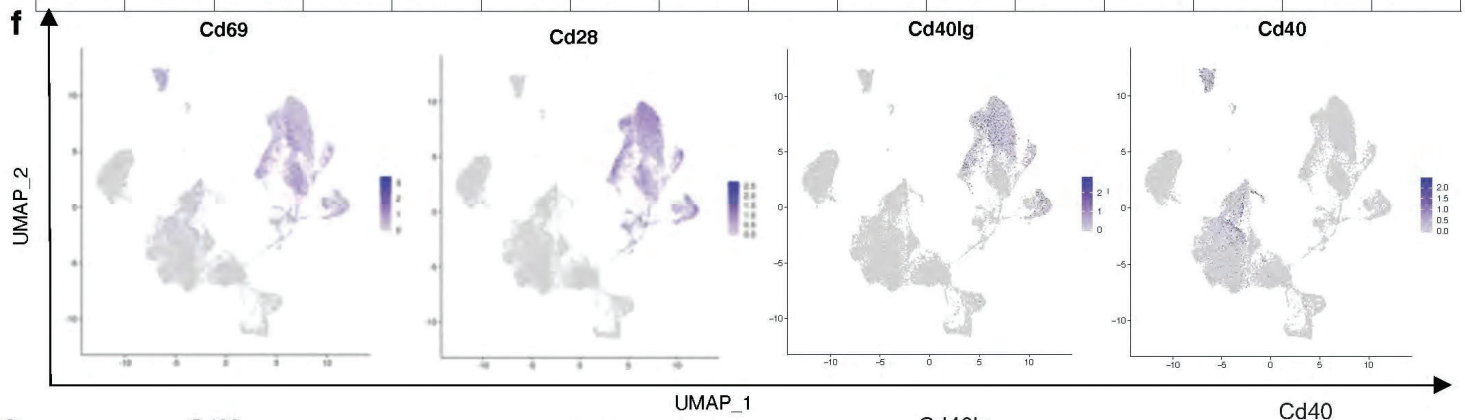

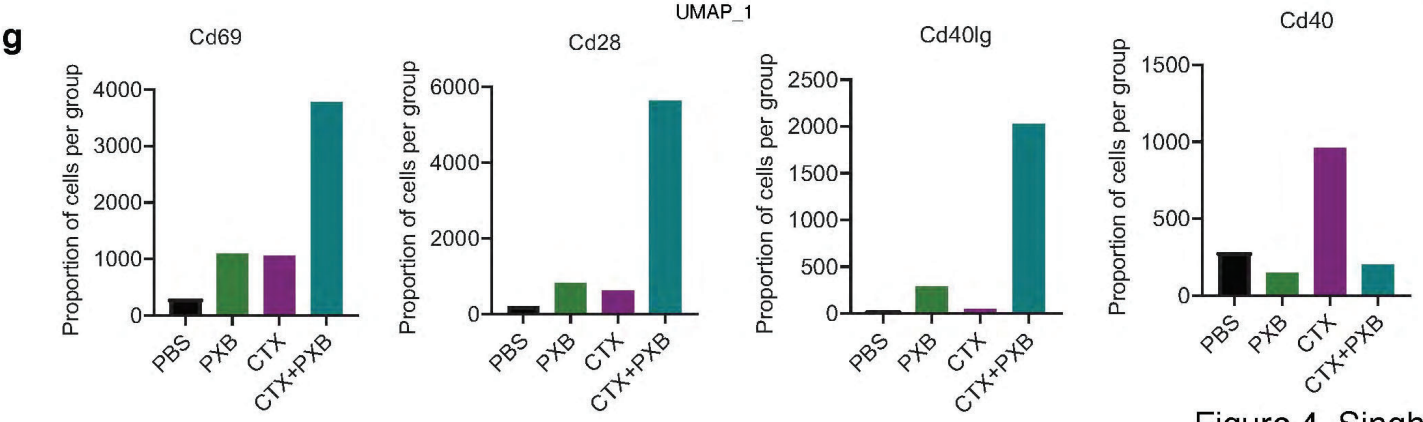

Figure 4, Singh et al.

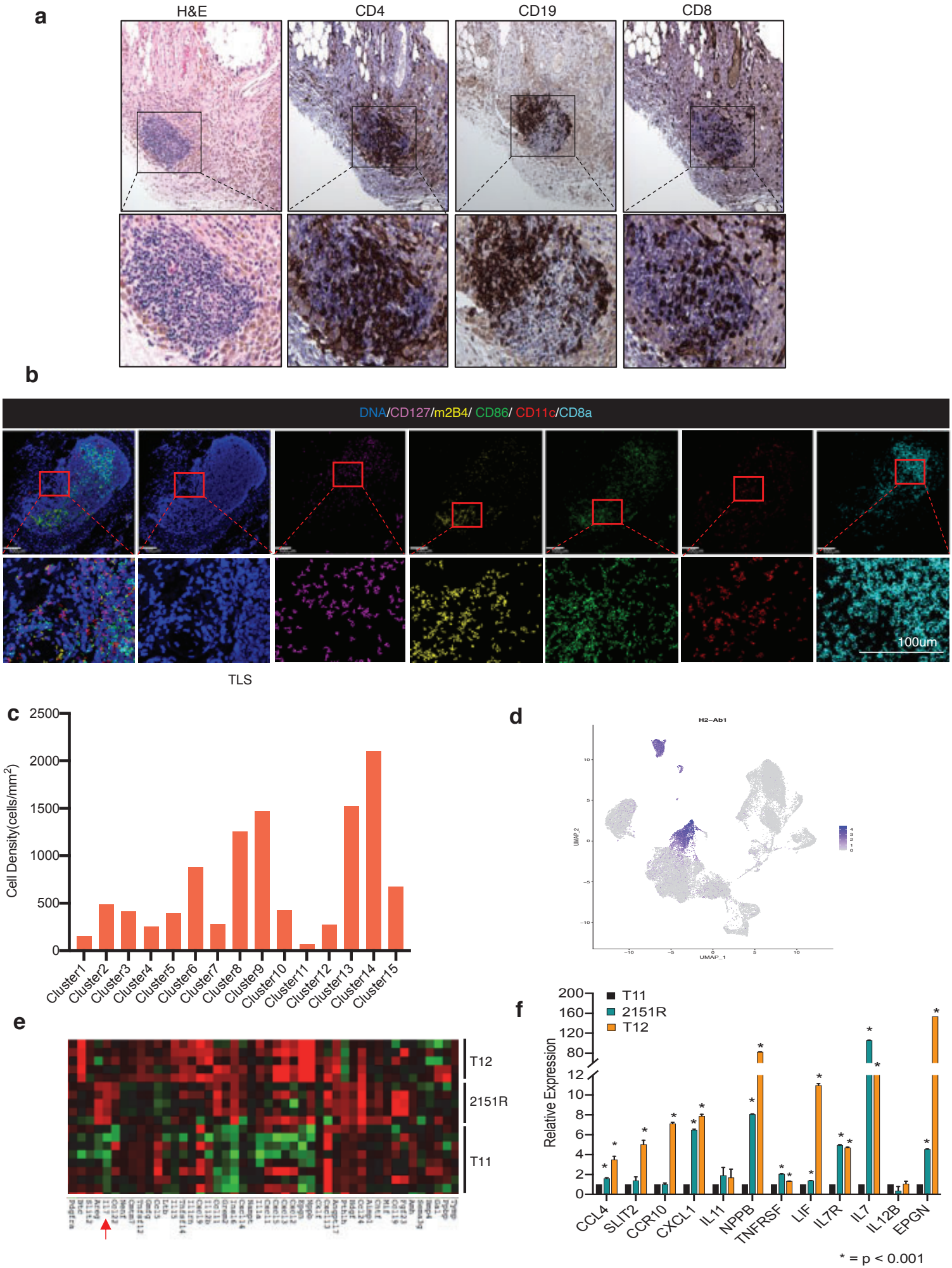

Supplementary Figure 4 for Figure 4 Singh et al.

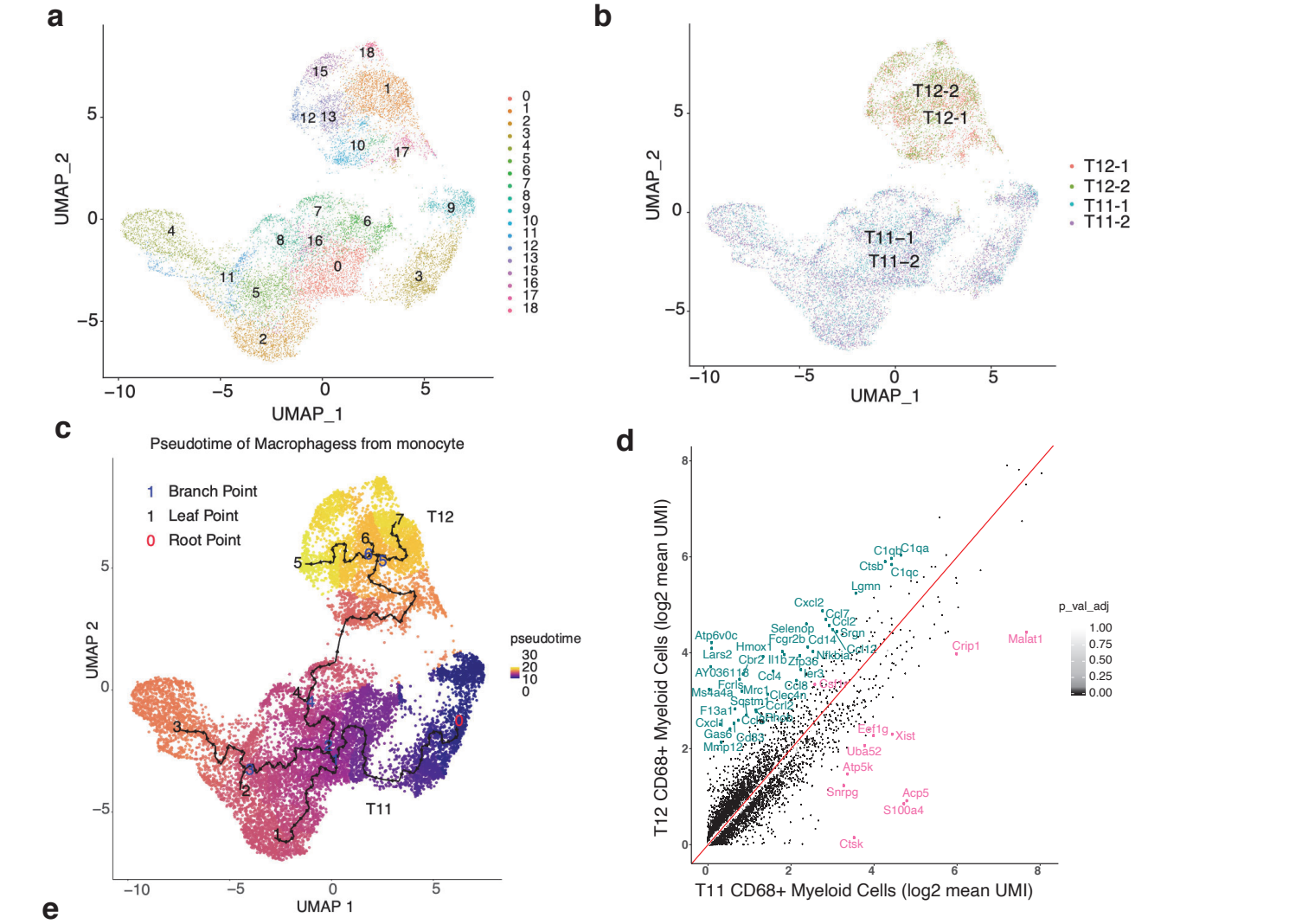

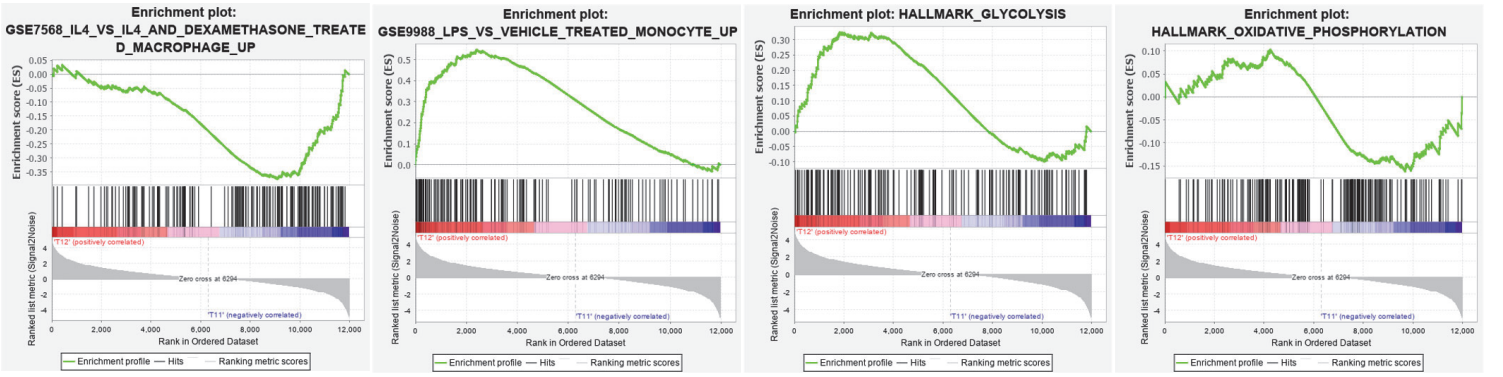

Figure 5 Singh et al.

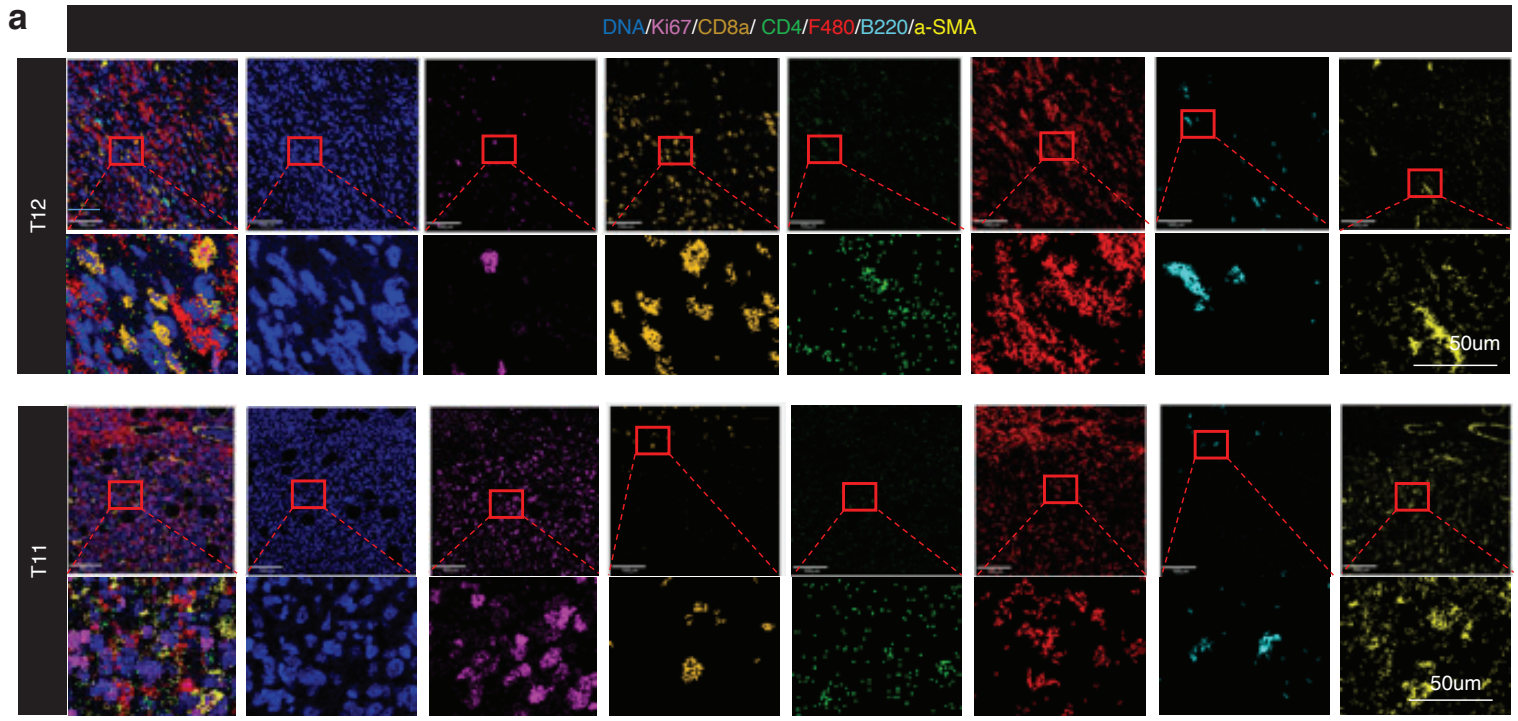

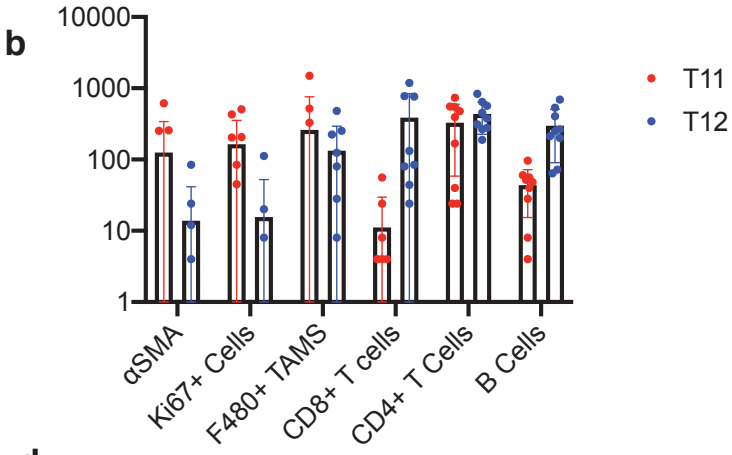

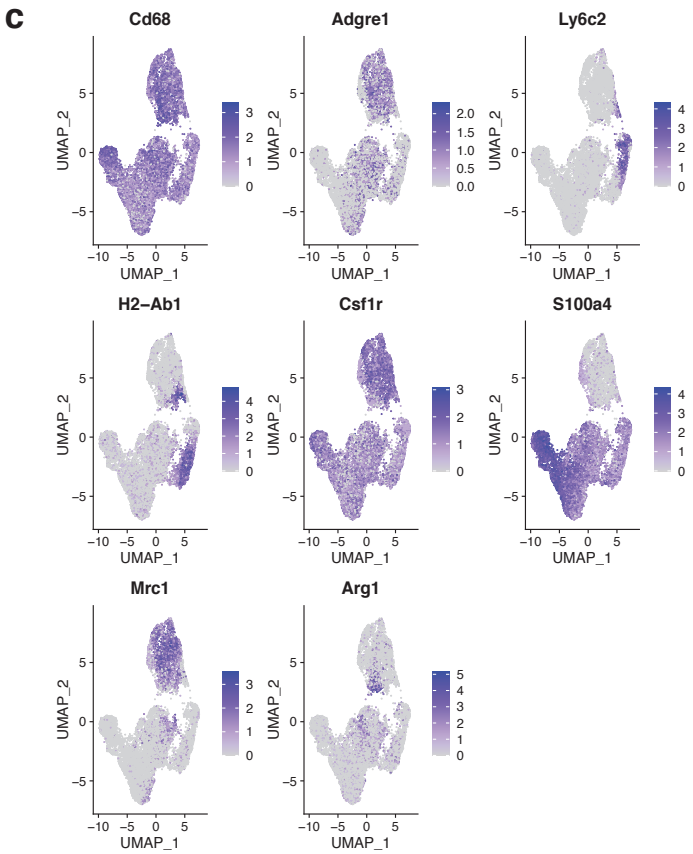

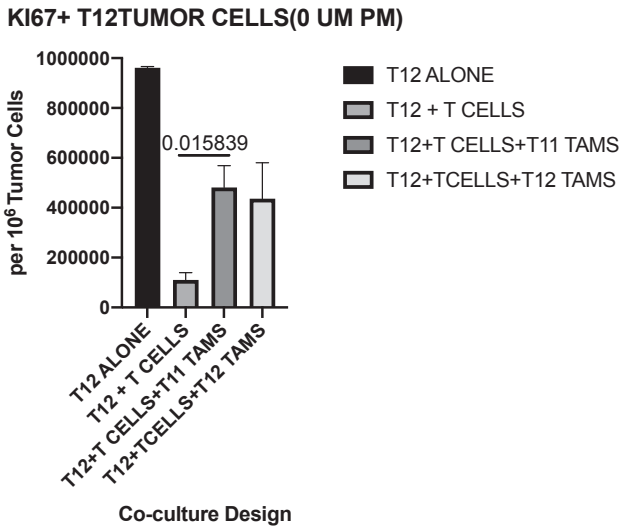

Supplementary Figure 5 for Figure 5 Singh et al.

a

All Triple Negative Breast cancer

T12vsT11 Signature

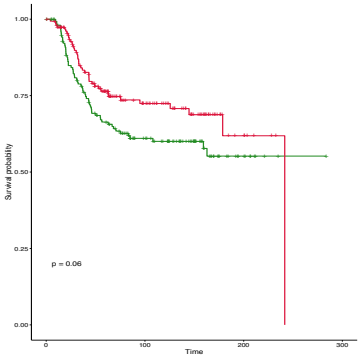

T11vsT11 Signature

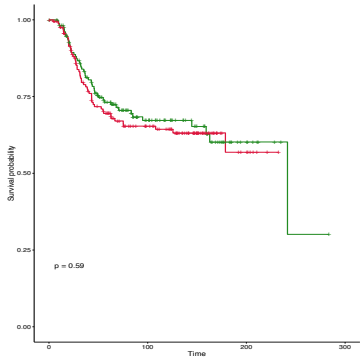

High

Low

b

TNBC-Chemotherapy Treated

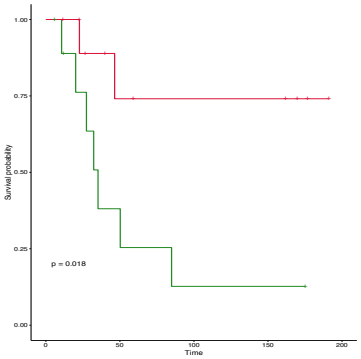

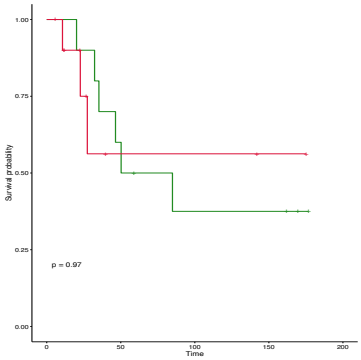

TNBC-Untreated

c

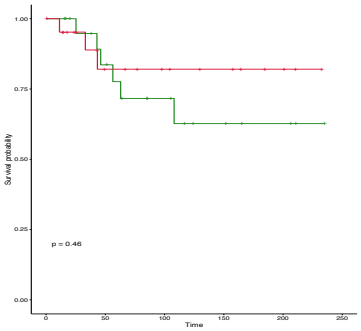

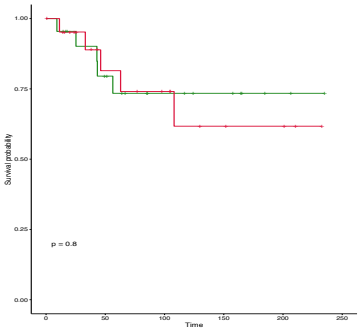

d

Patients with pCR (Pathologic Complete Response)

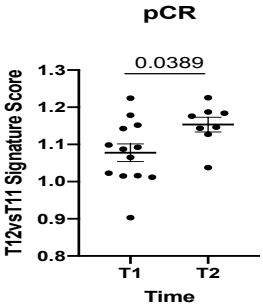

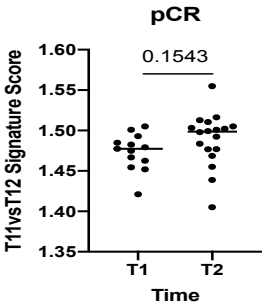

Patients with RD (Residual Disease)

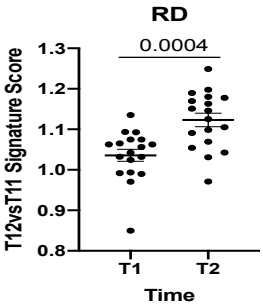

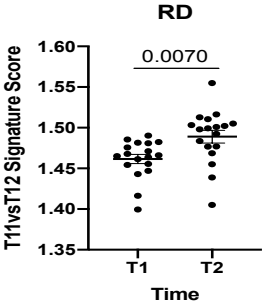

Figure 6, Singh et al.

a

All Breast cancer subtypes

T12vsT11 Signature

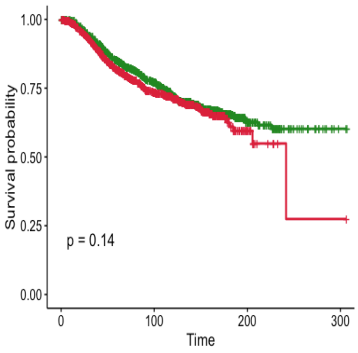

T11vsT11 Signature

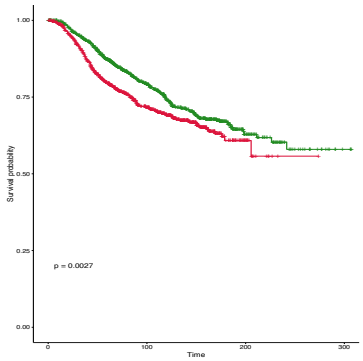

High

Low

Supplemental Figure 6 for Figure 6, Singh et al.

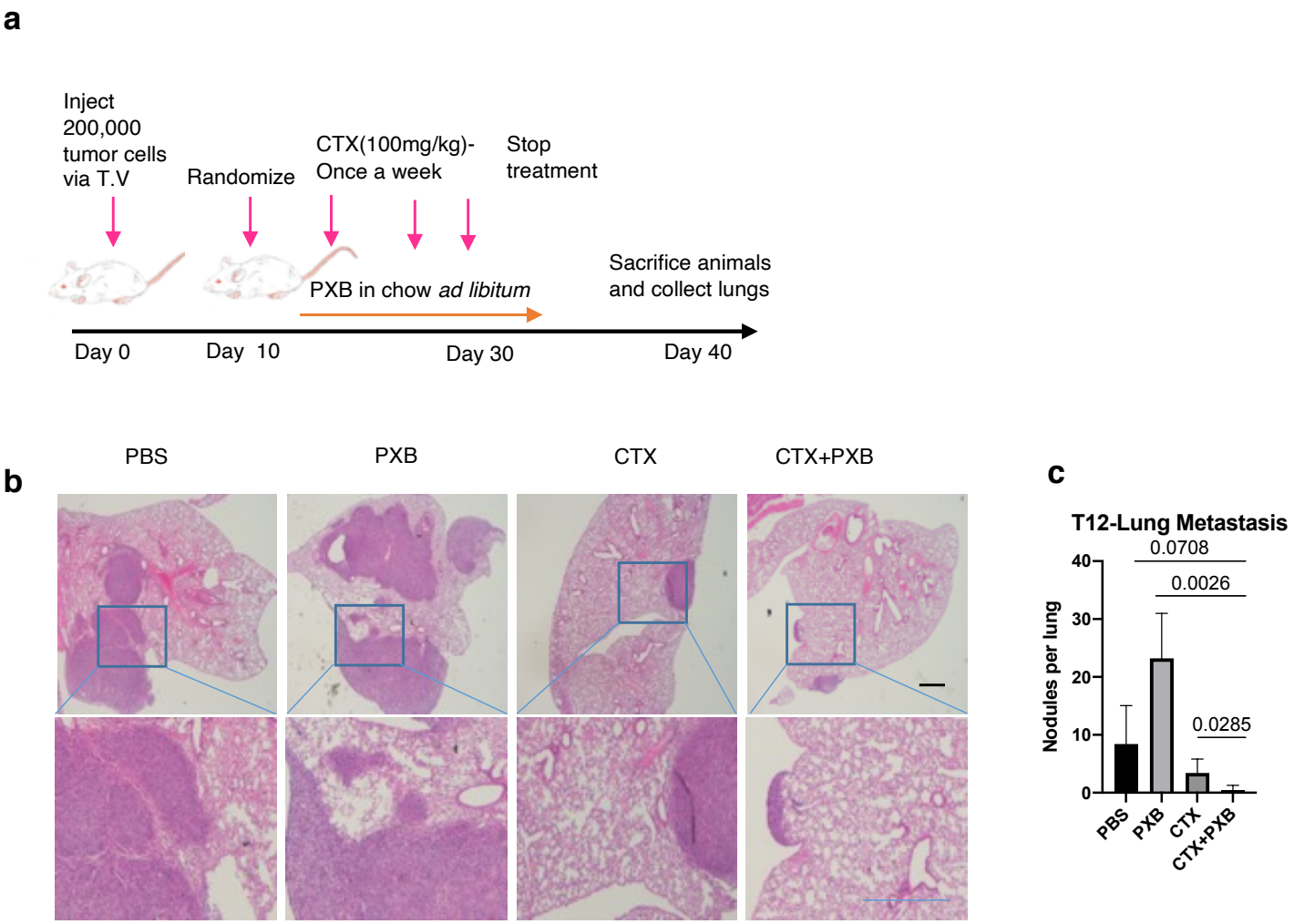

Figure 7, Singh et al.